DIELECTRIC MEASUREMENT

Dielectric measurements are concerned with the characterization of solid, liquid, and gaseous insulating materials over a wide range of dc and ac conditions at different frequencies, temperatures, field strengths, and pressures, under differing environments. The frequency range covered extends downward from the power frequency of 50 or 60 Hz through the ultra low frequency range of 10^{-2} to 10^{-6} Hz to dc and upward into the audio frequency (AF), radio frequency (RF) and microwave ranges and, finally, into the optical region for optically transparent dielectrics. It can be appreciated that a variety of specimen cells are required to suit the nature of the test and to act as containment vessels or holders for the specimens undergoing evaluation. The test methods and specimen containers used over the lower frequency spectrum differ substantially from those employed over the higher frequency spectrum (>300 MHz), because, at lower frequencies, the dielectric specimen behaves as a lumped circuit element, as opposed to its distributed parameter behavior over the higher frequency region, where the physical dimensions of the specimen become of the same order as the wavelength of the electrical field. This delimiting difference necessarily requires other test procedures to be utilized at high frequencies, and constitutes perhaps the main reason for the bifurcation and the unfortunate, but often attending, isolation of the two fields of endeavor—even though the aim over the lower and upper frequency regions is identical, namely, the characterization of dielectric materials.

Space does not permit a detailed description of all the dielectric measurement procedures and, consequently, only a cursory presentation is made. Nor is it possible, within the given constraints, to delve into the various dielectric conduction and loss mechanisms in order to discuss the interpretative aspects of the measurement methods. Accordingly, the presentation is necessarily confined to a concise description of the most common methods of dielectric measurement employed currently. Wherever feasible, the methods given attempt to comply with the general guidelines of those specified in national and international standards, such as those by ASTM (American Society for Testing and Materials) and IEC (International Electrotechnical Commission), in order to put methods forward that are universally accepted and have withstood the test of time. The dielectric measurement methods presented here will deal principally with those of dc conductivity, dielectric constant and loss as a function of frequency, and voltage breakdown or dielectric strength.

DC CONDUCTIVITY MEASUREMENTS

Volume Resistivity, ρ_v

Insulating materials employed on electrical equipment are usually characterized by a high insulation resistance and thus provide an isolating medium between adjacent components that are maintained at different potentials. In certain applications, such as for capacitor components, bushings, and cables, they must exhibit extremely low leakage current. In other applications, where partially conducting polymers are of interest, the insulation resistance values are substantially reduced. Insulation resistance measurements, which are generally carried out under dc conditions, yield not only data on

the electrical conduction characteristics of a material, but may also provide an indication of the uniformity or impurity content of the insulating material. It is thus of considerable practical interest to classify the various insulating materials in terms of their dc insulation resistance, which can then be related to their dc electrical conductivity. The dc conductivity, σ_{dc}, of an insulating or dielectric material, is a more fundamental property, as it bears a direct relationship to the conduction mechanisms taking place in the dielectric. It is defined as (1)

$$\sigma_{dc} = \frac{J_{\ell dc}}{E} \tag{1}$$

where $J_{\ell dc}$ is the dc leakage or conduction current density in $A\ cm^{-2}$ and E is the direct electrical field in $V\ cm^{-1}$; the units of σ_{dc} are in $S\ cm^{-1}$. If it is assumed that the dc conductivity arises from a drift of singly charged carriers, e, in the field direction, having a charge concentration n per cm^3 and a mobility of μ in $cm^2\ V^{-1}s^{-1}$, then Eq. (1) may be expressed as

$$\sigma_{dc} = e\mu n \tag{2}$$

The measured dc volume insulation resistance, R_v, is related to the dc volume resistivity of dielectric, ρ_v, by

$$\rho_v = \frac{A}{d} R_v \tag{3}$$

where A is the area of the measuring electrodes in cm^2 and d denotes the thickness of the dielectric specimen in cm; by definition, the dc conductivity is inversely related to the dc volume resistivity as,

$$\sigma_{dc} = 1/\rho_v \tag{4}$$

such that the units of volume resistivity are in Ω cm.

There are various specimen-holder electrode systems and measurement techniques available for determining the volume insulation resistance, R_v, in terms of which the volume resistivity, ρ_v, may be computed, employing Eq. (3) (2–4). For illustrative purposes, only the most prevailant ones in use will be considered. Figure 1 depicts a typical three-terminal

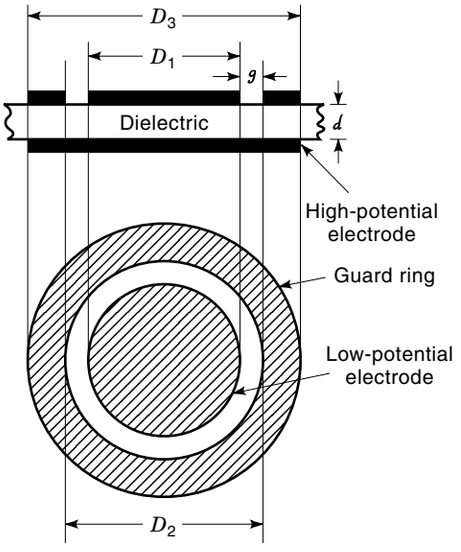

Figure 1. Three-terminal electrode system for the measurement of volume resistivity (after ASTM D257) (3).

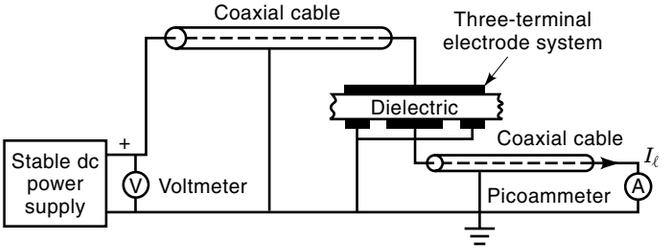

Figure 2. Schematic circuit diagram for a three-terminal measurement of the volume insulation resistance.

electrode system with the dielectric specimen held between circular parallel-plane metallic electrodes. The electrodes are usually made of stainless steel, with the low-potential (guarded) electrode of diameter D_1, having a diameter size less than the high-potential electrode, whose diameter D_3 is equal to that of the guard ring electrode. The separation between the latter and the low-potential guarded electrode is equal to g, such that $g \leq 2d$, where d denotes the thickness of the dielectric specimen. The gap g between the low-potential and guard electrodes must be sufficiently large to prevent leakage over the surface of the dielectric from influencing the volume resistivity measurement; this is particularly important with high-input impedance electrometers. A value of $g = 2d$ is most expedient, since it permits the measurement of both volume and surface insulation resistance with an identical electrode configuration.

The fringing of the flux lines essentially extends the guarded electrode edge into the gap region bounded by the measuring or low-potential electrode and the guard ring. Hence the area, A, in Eq. (3) is not the geometrical area of the low-potential electrode, but is approximately given (2) by

$$A = \frac{\pi (D_1 + g)^2}{4} \tag{5}$$

The determination of specimen thickness, d, in Eq. (3), does not present itself as a trivial problem (5). Exact parallelism between the two opposite sides of a solid dielectric specimen is difficult to achieve, in practice. With polymers, it is common to make several thickness measurements along the specimen surface, either with a micrometer or a dial gage, and then determine the average value of d. With most polymeric materials, the dielectric specimens will tend, in general, to conform to the surface of the measuring electrodes. However, with hard materials, the optically flat electrodes will generally not be contiguous with every portion of the surface of the dielectric. In such circumstances, the three-terminal electrodes must be either paint or vapor deposited upon the rigid surfaces of the specimen. For this purpose, silver or aluminum is frequently employed, though aluminum is less desirable, because of its propensity to form nonconducting oxide films. Alternatively, tin foil electrodes may be utilized, in conjunction with a minute thickness of silicone grease, applied to ensure their adhesion to the specimen's surface. When liquid dielectrics are evaluated, permanently mounted three-terminal electrodes are employed, in conjunction with a cell container into which the liquid specimen submerges the measurement electrodes.

Figure 2 portrays a schematic three-terminal circuit diagram for the measurement of the volume insulation resis-

tance, R_v. Perhaps one of the most important considerations in the measurement of R_v is the time at which, following the application of the electrical field, the actual measurement is made. When the voltage is suddenly applied across the specimen, the observed initial charging current is associated with the polarization of the dielectric; both the induced and permanent dipoles in the dielectric become aligned in the direction of the electrical field. Once this very rapid process is completed, the current commences a monotonic decline with time, as surplus free charge carriers are gradually swept out of the dielectric by the electrical field. The nature of these charge carriers and their mobility are directly associated with the structure of the dielectric material. If the dielectric has an open structure, such as glass, the charge carriers may be ions; similarly, in a dielectric liquid such as an oil, where electrolytic contamination may be the source of the charge carriers, ions may be also responsible for the conduction current. In polymers, where the latitude of ionic motion is greatly restricted, the conduction process is frequently governed by electrons. Ideally, the R_v value should be measured when the conduction or the so-called leakage current attains a constant value, which is a function of the dielectric under test. For example, in a polymer, the value of constant current may be achieved when all excess free electrons have been removed from the dielectric and the residual leakage current is entirely determined by the trapping and detrapping rates of the electrons at the various traps (principally shallow traps). That is, the number of migrating electrons at any one time approaches a constant value when an equilibrium is attained between the time each electron resides trapped in a well and the time it is free to migrate before it becomes again retrapped. Since the complexity of the conduction process virtually ensures that different dielectrics are characterized by different times necessary for the leakage current to attain a constant value, it has been agreed *ad arbitrium* that all insulation resistance measurements should be made following a one-minute application of the electrical field.

Since the volume resistivity, ρ_v, of good insulating materials falls in the range of 10^{12} to $>10^{18}$ Ω cm, the leakage current, I_ℓ, for such materials must be measured with a picoammeter, as indicated in Fig. 2. The guard circuit improves the accuracy of the measurement by reducing the influence of the leakage resistance. The effects of the coaxial cable resistance connected across the dc power supply can be greatly decreased by shunting the input of the coaxial cable to its shield, by means of an operational amplifier with unity gain; this feature is often incorporated in commercially available electrometer/ohmmeter instruments (6).

The volume insulation resistance, R_v, in addition to being contingent upon the time of the voltage application, is also a function of the applied voltage, V; it is temperature dependent as well. Thus, the value of V and the temperature must be specified; in general, the values of 100 and 500 V are most commonly employed (2,3). Following one minute of voltage application, the value of R_v is then calculated from

$$R_v = \frac{V}{I_\ell} \tag{6}$$

In the measurement of R_v an accuracy of 5% may be readily obtained. However, as the volume resistivity, ρ_v, is subsequently obtained in terms of Eq. (3), the accuracy of the ρ_v value is somewhat degraded, as a result of errors inherent in the measurement of the specimen thickness, d, and the estimation of the electrode area A [refer to Eq. (5)] when compensation for the field fringing effects is made.

Surface Resistivity, ρ_s

Surface resistance, R_s, of solid insulating materials is, to a large extent, determined by the state of cleanliness or contamination of the surface of the dielectric under test. It is, as well, a strong function of surface moisture, particularly if the moisture film contains electrolytic impurities either intrinsic to the liquid film itself or as a result of solid ionic contaminants originally present on the solid dielectric surface. Surface resistance is thus a measure of the material's propensity to surface contamination and constitutes a useful indicator as concerns the surface tracking resistance of insulators when subjected to electrical fields. It is common practice to condition the specimens prior to measurement in a dry atmosphere, before performing the actual measurement at 50% relative humidity.

Surface resistance measurements may be carried out, either with two- or three-terminal electrode systems, though most often three-terminal electrodes are employed to eliminate stray leakage effects. The units of surface resistance are ohms or ohms per square. The latter refers to the arrangement of the electrodes, the configuration of a square, on the surface of the specimen, as depicted in Fig. 3 (2).

It is evident from the electrode arrangement in Fig. 3 that the surface resistance measurement also includes a contribution of the volume resistance. The magnitude of this contribution diminishes as the surface conductivity becomes increasingly greater than the volume conductivity. The procedure followed in measuring the surface resistance, R_s, is identical to that of R_v. The surface resistance is given by

$$R_s = \frac{V}{I_{s\ell}} \tag{7}$$

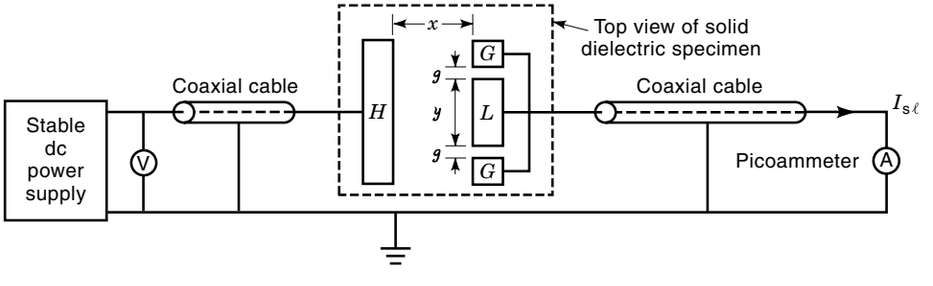

Figure 3. Schematic circuit diagram for the measurement of surface resistance with a three terminal electrode arrangement on the dielectric's surface (2).

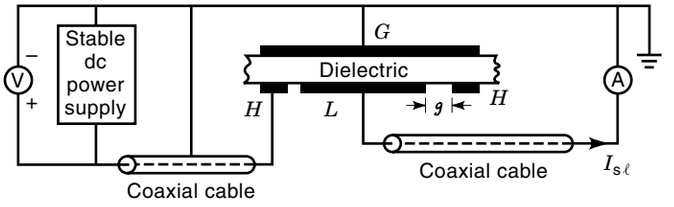

Figure 4. Schematic circuit diagram of a three-terminal circular electrode arrangement for the measurement of the surface insulation resistance (3,6).

where $I_{s\ell}$ is the surface leakage current and V is the voltage across the high-potential (H) and low-potential (L) electrodes. In Fig. 3, G represents the guard electrodes, and g denotes the separation between the guard (G) and low-potential (L) electrodes. The surface resistivity, ρ_s, in ohms or ohms per square, is then determined from (2)

$$\rho_s = \frac{y}{x} R_s \tag{8}$$

where y denotes the length of the low-potential electrode (L) and x is the separation between the high- (H) and low- (L) potential electrodes. The electrodes may be applied with silver paint; alternatively, silver or aluminum electrodes may be deposited upon the surface under vacuum. Frequently, tin foil electrodes are utilized with an extremely thin layer film of silicone jelly applied upon their underside, in order to provide adhesion upon the specimen's surface.

Another approach is to employ the circular three-terminal electrode system of Fig. 2, but with the connections changed as portrayed in Fig. 4. Note that with this arrangement, the high potential is applied to the circular electrode (H) encompassing the center electrode, which acts as the low-potential electrodes (L), while the upper electrode is connected to ground. In contradistinction to Fig. 2 (for volume resistivity measurements), the gap distance $g \geq 2d$; in analogy to Fig. 3, g is equivalent to the electrode separation distance, x. With circular electrode symmetry, the surface resistivity becomes (2,3)

$$\rho_s = \frac{\pi D_1}{g} R_s \tag{9}$$

where D_1 is the diameter of the low-potential electrode (L). The diameter of the upper grounded electrode (G) may be equal to or greater than that of the encompassing circular high-potential electrode (H).

PERMITTIVITY AND LOSS MEASUREMENTS ON LUMPED CAPACITANCE SPECIMENS

Under alternating voltages, dielectric materials are employed either as supports to insulate electrical components from each other and ground, or as dielectrics in capacitors. Some applications require dielectrics of low loss and low dielectric constant, while in others, high dielectric constant materials are desirable, to provide the highest possible capacitance for a given physical size. Thus two of the most important electrical properties of dielectric materials, in terms of which their use and application suitability at either low or high frequencies are assessed, are those of dielectric loss and dielectric constant.

The capacitance, C, of a parallel plate capacitor containing a dielectric material having a relative real permittivity, ϵ_r', may be expressed as

$$C = \epsilon_r' C_0 \tag{10}$$

where C_0 is the capacitance in vacuo and is given by

$$C_0 = \frac{\epsilon_0 A}{d} \tag{11}$$

where A is the area of the capacitor's plates in cm^2, d the thickness of the dielectric, and ϵ_0 the permittivity in vacuo equal to $8.854 \times 10^{-14}\ F\ cm^{-1}$. By definition, ϵ_r' is equal to the ratio ϵ'/ϵ_0, where ϵ' is the real value of the permittivity. Frequently, the relative real value of the permittivity, ϵ_r', is simply referred to as the dielectric constant. The occurrence of loss in dielectrics, which may be associated with the migration of free charge carriers, space charge polarization, or the orientation of permanent dipoles, is manifest externally by a phase shift between the electric field ($\boldsymbol{E}$) and the displacement ($\boldsymbol{D}$) vectors (1); consequently, the permittivity, ϵ, becomes a complex quantity of the form

$$\epsilon = \epsilon' - j\epsilon'' \tag{12}$$

where ϵ'' denotes the imaginary value of the permittivity. The total current density vector, $\boldsymbol{J}$, through the dielectric, composed of the leakage current density, $\boldsymbol{J}_\ell$, and capacitative or displacement current density, $\boldsymbol{J}_c$, vectors, may be expressed in terms of ϵ' and ϵ'' as

$$\begin{aligned} \boldsymbol{J} &= \boldsymbol{J}_\ell + \boldsymbol{J}_c \\ &= (\omega\epsilon'' + j\omega\epsilon')\boldsymbol{E} \end{aligned} \tag{13}$$

The phasor relationship between the current density vectors $\boldsymbol{J}_\ell$, $\boldsymbol{J}_c$ and $\boldsymbol{J}$ is delineated in Fig. 5(a) with its corresponding RC equivalent circuit in Fig. 5(b), in terms of which the dissipation factor, tan δ, of the dielectric specimen may be defined as

$$\tan\delta = \frac{\boldsymbol{J}_\ell}{\boldsymbol{J}_c} = \frac{\boldsymbol{I}_\ell}{\boldsymbol{I}_c} \tag{14}$$

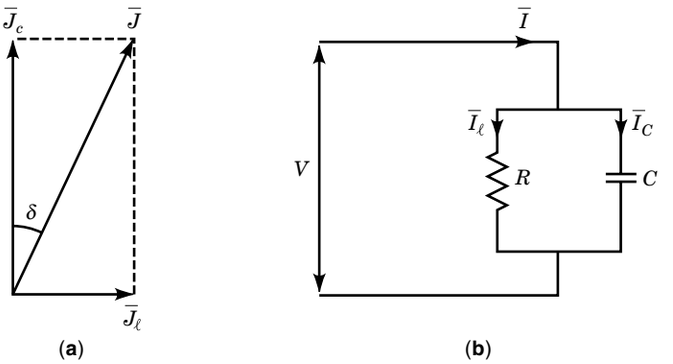

Figure 5. Current density phasor relationship in a dielectric (a) with its corresponding equivalent parallel RC circuit (b).

where $\boldsymbol{I}_\ell$ and $\boldsymbol{I}_c$ are the corresponding current vectors. From Eqs. (14) and (15), it follows that

$$\tan\delta = \frac{\epsilon''}{\epsilon'} \tag{15}$$

Since the ac conductivity, σ_{ac} is by definition, equal to $\boldsymbol{J}_\ell/\boldsymbol{E}$, then, in terms of Eq. (13),

$$\sigma_{ac} = \omega\epsilon'' \tag{16}$$

and

$$\tan\delta = \frac{\sigma_{ac}}{\omega\epsilon'} \tag{17}$$

The ac conductivity, σ_{ac}, must be distinguished from its dc value, σ_{dc}, because it may include permanent dipole orientation losses, as well as frequency-dependent space charge polarization controlled carrier migration processes, which do not arise under dc conditions. It is readily apparent from the equivalent circuit diagram, which represents the lossy part of a dielectric by an equivalent resistance, that

$$\begin{aligned}\tan\delta &= \frac{\boldsymbol{I}_\ell}{\boldsymbol{I}_c} \\ &= \frac{1}{\omega RC}\end{aligned} \tag{18}$$

where $\boldsymbol{V}$ is the applied voltage vector and I_ℓ is given by $\boldsymbol{V}/R$ and $\boldsymbol{I}_c$ by $j\omega C\boldsymbol{V}$. It must be borne in mind that the parallel equivalent RC circuit representation in Fig. 5(b) is valid only at one particular frequency, since both R and the capacitance, C, of the specimen are functions of frequency, as well as temperature and electrical field. It must be further emphasized that, whereas some dielectric measurement circuits view the dielectric specimen as a parallel equivalent circuit with a large equivalent parallel insulation resistance R, others consider the dielectric as a series RC circuit, where the series resistance, $R_s \ll R$. The tan δ value for the series RC circuit representation becomes

$$\tan\delta = \omega R_s C \tag{19}$$

It is apparent that one can derive the primary dielectric parameters of σ_{ac}, ϵ'' and ϵ' from the measured values of C and tan δ by means of Eqs. (10), (15), and (17).

Measurements at Low Frequencies (10^{-6} to 10 Hz)

In studies related to the identification of charge carriers and space charge effects, it is desirable to carry out measurements in the frequency range between 10^{-6} and 10 Hz. For measurements below 10^{-1} Hz, it is common practice to apply a rapid rise time voltage step pulse across the specimen and subsequently observe the form of the charging or decay current. The arrangement for this measurement is very similar to that of the volume resistivity measurement in Fig. 2, with the exception that a switch is employed in conjunction with the dc power supply to abruptly apply a voltage step across the specimen (7,8). Since the total charging current comprises all the frequency components contained within the voltage excitation step, Fourier transformation procedures can be utilized to derive the individual current distributions at the discrete frequencies. This procedure may be utilized irrespective of whether the specimen is charged or discharged. The relative real and imaginary permittivities, ϵ_r' and ϵ_r'', respectively, may be expressed in terms of the resulting current as

$$\epsilon_r'(\omega) = \frac{1}{C_0 V}\int_o^\infty i(t)\cos\omega t\,dt + \frac{C_\infty}{C_0} \tag{20}$$

and

$$\epsilon_r''(\omega) = \frac{1}{C_0 V}\int_o^\infty i(t)\sin\omega t\,dt + \frac{G}{\omega C_0} \tag{21}$$

where V is the magnitude of the voltage step, C_∞ represents the lumped capacitance of the specimen at infinite frequency and G is the dc conductance. Practical implications impose the upper and lower integration limits on Eqs. (20) and (21); the lower limit is fixed by the rise time of the electrometer employed (usually about 1s) and the upper limit by the smallest value of current that the electrometer can measure (about 10^{-16} A) in the presence of extraneous noise. A numerical procedure is normally followed, to carry out these types of measurements (9). For each frequency of measurement, the computer performs a numerical integration between the two integration limits to determine the values of ϵ_r' and ϵ_r''.

An automated precision time-domain reflectometer procedure is available, which permits rapid measurements down to 10^{-4} Hz with an accuracy of 0.1 percent and a resolution of 10^{-5} in the tan δ value (10,11). Its schematic circuit diagram is depicted in Fig. 6.

Positive and negative voltage steps are applied across the specimen and the reference capacitors, C and C_{ref}, respectively. The operational amplifier, in conjunction with the feedback capacitor, C_f, constitute a charge detector, providing an output, which is proportional to the net charge injected $[Q_{ref} - Q(t)/C_f]$ by the two opposite polarity voltage steps of amplitude ΔV and $-\Delta V$, respectively. As the voltage across the specimen changes from 0 to ΔV, the charge, $Q(t)$, flowing through the specimen is determined from

$$C(t) = Q(t)/\Delta V \tag{22}$$

where $C(t)$ denotes a time-dependent capacitance. Hence the complex capacitance of the specimen $C^*(\omega)$, as a function of frequency, may be expressed as

$$\begin{aligned}C^*(\omega) &= C'(\omega) - jC''(\omega) \\ &= \int_o^\infty C(t)'\exp[-j\omega t]\,dt\end{aligned} \tag{23}$$

where $C(t)'$ is the time derivative of $C(t)$. The relative real and imaginary permittivities, ϵ' and ϵ'', are then deduced from

$$C'(\omega) \simeq \int_o^\infty C(t)\cos\omega t\,dt + C(0) + C_{ref} \tag{24}$$

and

$$C''(\omega) \simeq \int_o^\infty C(t)\sin\omega t\,dt \tag{25}$$

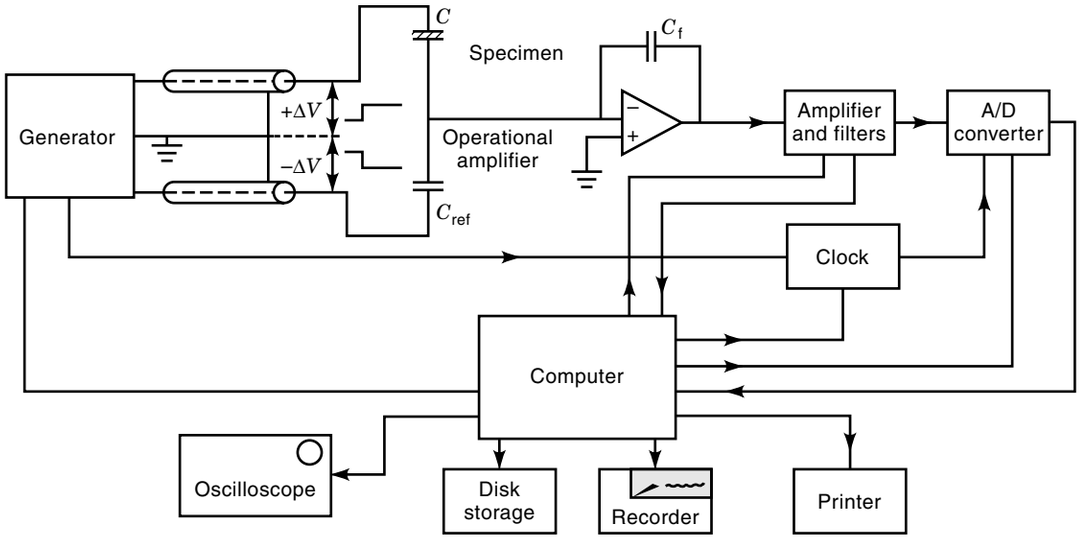

Figure 6. Schematic circuit diagram of time-domain system for measurements down to 10^{-4} Hz (10).

where $C'(\omega)$ and $C''(\omega)$ are the real and imaginary capacitances corresponding to $\epsilon_r' C_0$ and $\omega\epsilon_r'' C_0$, respectively; $C(0)$ is the initial capacitance and the integration is carried out for all times following the application of the voltage step at $t = 0$. The minimum and the maximum feasible measurement times t_{max} and t_{min} determine the minimum and maximum measurement frequencies $\omega_{min}/2\pi$ and $\omega_{max}/2\pi$, respectively. The entire measurement is completed in less than one cycle at $\omega_{min}/2\pi$.

A most useful instrument, which is frequently employed in the range from 10^{-2} to 10^2 Hz and occasionally up to 10^4 Hz, is the Thompson–Harris bridge (12,13). A two-terminal specimen cell is utilized in conjunction with the bridge, so that a correction must be made to take into account fringing effects at the electrode edges. The schematic circuit diagram of the bridge, portrayed in Fig. 7, incorporates a specimen biasing feature (14), which is included to permit the determination of the depth of charge traps in the dielectric bulk and adjacent to the measuring electrodes.

The highly regulated frequency generator used in conjunction with the Thompson–Harris bridge must provide exact in-phase and quadrature voltage outputs of V and jV, respectively. Operational amplifiers delineated in Fig. 7 provide the necessary voltage, phase, and impedance relationships. The capacitive current of the specimen is balanced by the injection of an out-of-phase voltage, $-\beta V$, across a variable capacitor, C_c; injection of a quadrature voltage of αjV across C_R compensates for the conduction or leakage current in the specimen conductance, G_x. Balance of the bridge is achieved by manipulating the capacitors C_C and C_R and observing the null point, in terms of the Lissajous figures displayed on the long-persistence oscilloscope. At balance, the conductance of the specimen, G_x, is given by

$$G_x = \omega\alpha C_R \tag{26}$$

and the capacitance of the specimen, C_x, is

$$C_x = \beta C_c \tag{27}$$

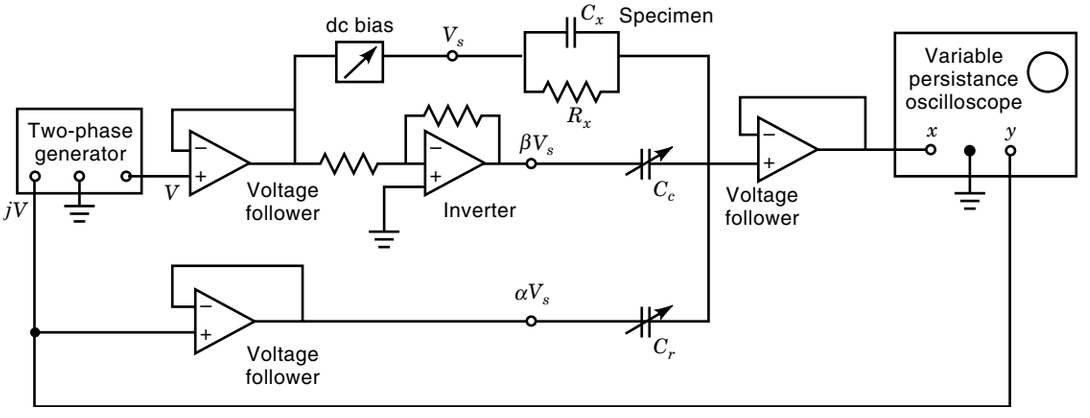

Figure 7. Thompson–Harris low-frequency bridge with specimen bias control feature (14).

from which the dissipation factor of the dielectric, tan δ, is obtained as

$$\tan\delta = \frac{G_x}{\omega C_x} = \frac{\alpha C_R}{\beta C_c} \tag{28}$$

Note that α and β are dimensionless quantities, representing the fraction of the voltage, V_s injected across C_R and C_c, respectively.

Not indicated in Fig. 7 is a zero offset feature, which is utilized in routine measurements to compensate for the dc coupling circuitry, in order to prevent erratic shifts in the Lissajous figures while balancing is being carried out. The accuracy of the bridge is 0.1% with resolution ordinarily better than 0.1%.

Frequency response analyzer methods may also be employed for low-frequency measurements. These computerized techniques perform adequately well within the range of 10^{-4} to 10^4 Hz (15).

Power and Intermediate Frequency Methods (10 Hz–1 MHz)

A considerable portion of the electrical insulating materials manufactured for use in electrical apparatus and cables are evaluated within the frequency range from 50 Hz to 1 MHz, employing primarily bridge type circuits. A further substantial portion of tests at high voltages are carried out at fixed power frequencies of 50, 60, and 400 Hz. The bridge circuits designed for power frequency applications, where measurements are normally made as a function of voltage, differ significantly from those involving measurements as a function of frequency at low voltage. Since most of these tests are performed by means of either Schering or transformer ratio arm bridges, the discussion here will be essentially confined to these types of bridges.

A common low-voltage Schering bridge arrangement, which employs the parallel substitution technique recommended in ASTM D150 (16), is depicted in Fig. 8 for the case where measurements are carried with a two-terminal specimen cell.

The capacitance C_3 is selected such that its negligibly small dielectric losses are approximately equal to those of the intrinsically low loss standard capacitor, C_s. Note that the Schering bridge views the specimen as an equivalent series R_xC_x device, so that the variable arm composed of the parallel combination of R_1 and C_1 must be capable of compensating for the losses in the small series resistance R_x of the specimen. The null detector, which is normally an amplifier, is tuned to the frequency of the measurement, $f = \omega/2\pi$. Balance is first obtained by an adjustment of the capacitors C_1 and C_s, with the specimen disconnected. Then with the specimen placed in parallel with the standard capacitor, C_s, the bridge is rebalanced. The specimen capacitance, C_x, is thus determined from

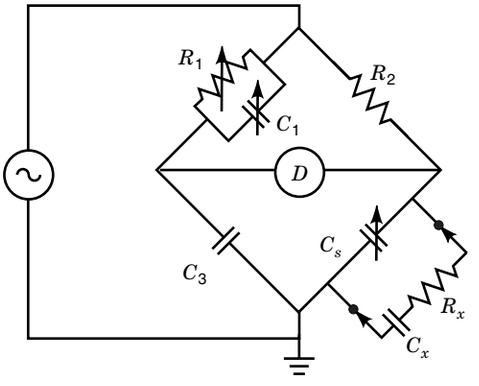

Figure 8. Low-voltage Schering bridge, employing the parallel substitution technique in accordance with ASTM D150 (16).

$$C_x = C'_s - C''_s \tag{29}$$

and the dissipation factor from

$$tan\delta_x = \frac{\omega R_1 C'_s (C''_1 - C'_1)}{(C'_s - C''_s)} \tag{30}$$

where C'_1, C'_s, and C''_1, C''_s denote the values of the variable capacitors C_1 and C_s at balance with the specimen disconnected and reconnected, respectively. The substitution technique eliminates the errors introduced by the coupling effects of the various stray capacitances, but it does not circumvent errors arising from connecting lead influences.

The procedures for the correction of lead and stray capacitance effects have been standardized and are explicitly enumerated in ASTM D150 (16). It is the inductance, L_s, and the resistance, R_s, of the leads, which contribute to the apparent increase of the capacitance, ΔC, and the dissipation factor, Δ tan δ, in accordance with the relations (16)

$$\Delta C = \omega^2 L_s C^2 \tag{31}$$

and

$$\Delta \tan\delta = \omega R_s C \tag{32}$$

where C is the true capacitance of the specimen; it is to be emphasized that, as the skin effect increases with frequency, the lead resistance R_s increases significantly with the square root of the frequency, $f = \omega/2\pi$. A standard practice for assessing the effect of the leads, is to perform a measurement on a miniature sized capacitor, with the latter being first directly connected to the bridge terminals and then inserted across the far end of the leads. The difference between the two readings permits the calculations of ΔC and Δ tan δ.

The appearance of an edge capacitance, C_e, and a ground capacitance, C_g, will lead to an increase in the measured apparent capacitance

$$C_a = C + C_e + C_g \tag{33}$$

and an apparent dissipation factor

$$\tan\delta_a = \frac{C\tan\delta}{C_a} \tag{34}$$

The relative real and imaginary permittivity, ϵ'_r and ϵ''_r, will then be given by

$$\epsilon'_r = C/C_0 = [C_a - (C_e + C_g)]/C_0 \tag{35}$$

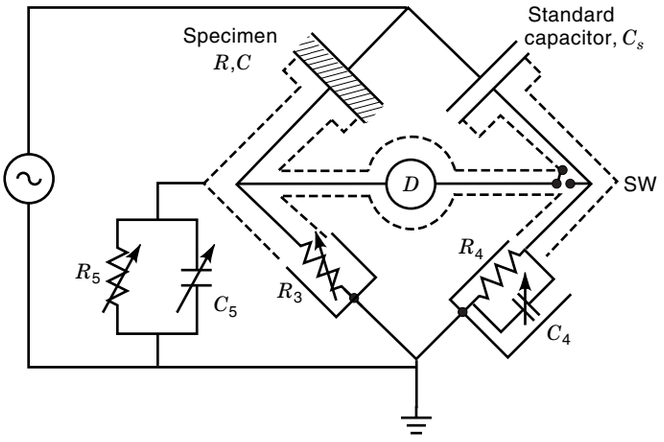

Figure 9. Classical power frequency circuit of high-voltage Schering bridge with Wagner's earth (2).

and

$$\epsilon_r'' = C_a \tan \delta_a / C_0 \tag{36}$$

For the normal type of specimen dimensions, where the parallel-plane cylindrical electrodes are smaller than the diameter of the specimen, the capacitance in vacuo, C_0, with edge effect correction, may be expressed empirically in pF as (16)

$$C_0 = 0.006954 \frac{D^2}{d} \tag{37}$$

where d is the thickness of the specimen and D the diameter of the electrodes in mm. Exact formulas for the edge correction may be found in (17); the use of the exact formulas does not result in a significant difference for the correction. As with all dielectric measurements, the accuracy attainable is contingent not only upon the accuracy of the observed capacitance and tan δ values, but also on the stray and edge effects of the electrodes employed, as well as the calculated interelectrode vacuum capacitance, C_0. In general, the permittivity is determinable to within $\pm$ 1% and the tan δ value to within $\pm$ (5% + 0.0005) (16)

The circuit of a power frequency high-voltage Schering bridge, portrayed in Fig. 9, represents essentially an inverse arrangement of its sibling low-voltage bridge equivalent. The lower bridge arms of R_4, C_4, and R_3 constitute the balancing elements, while the upper arms of the series representation of the specimen, R, C, together with the standard capacitor, C_s, which have a high impedance in comparison with the lower resistive arms, assume the major portion of the voltage drop. This arrangement provides the bridge with an inherent safety feature, since the lower arms where balance manipulation of the bridge is carried out, remain at low potential. Figure 9, which represents the classical Schering bridge circuit, delineates also the guard circuit's balancing elements R_5 and C_5, arranged in accordance with the so-called Wagner's earth method. The guard circuit, which is implemented in order to eliminate the stray capacitance to ground, necessarily entails the use of a three-terminal measurement procedure. The solid dielectric slab specimen is placed in a three-terminal cell of the type depicted in Fig. 1, or if the specimen is a liquid dielectric, a concentric coaxial electrode cell (18) may be employed. Frequently, the specimen undergoing test may be a high-voltage power cable or stator bar, whose high-voltage terminated ends must also incorporate a guard circuit (19). The standard capacitor, C_s, which must be partial discharge free up to the maximum measurement voltage, is normally a 100 pF compressed gas-filled unit with negligible dielectric loss. Note that the low-voltage arms are enveloped in grounded shields; the shield, screening the low-potential electrodes of the specimen and standard capacitor, including the detector that normally comprises an amplifier tuned to the power frequency, eliminates the stray capacitances to ground and between the components themselves. Thus, any capacitance current, which may develop between the detector and the high-voltage portion of the bridge, flows directly to ground via the auxiliary bridge arm of R_5 and C_5. Since the latter are interposed between the shield and the bridge ground, their manipulation balances the guard or shield circuit. The switch *SW*, shown in Fig. 9, permits the necessary independent balancing steps for the bridge guard circuit and the bridge itself. At balance, the capacitance of the specimen (2) is given by

$$C = \frac{C_s R_4}{R_3} \tag{38}$$

and for equal self-inductances inherent with the resistive elements R_3 and R_4, the dissipation factor reduces to

$$\tan \delta = \omega R_4 C_4 \tag{39}$$

Since high-voltage Schering bridges are normally designed to operate at one fixed power frequency, the dials of R_3 and C_4 are calibrated to read directly the capacitance and tan δ values of the specimen, respectively. It is to be emphasized that, under high voltage conditions, should the specimen under test undergo partial discharge, then the indicated tan δ value will reflect the power losses due to partial discharges, in addition to the dielectric losses occurring in the solid, liquid, or solid-liquid insulating system of the specimen (20).

Present high-voltage fixed power frequency Schering bridges employ a driven or active guard technique for balancing of the guard circuit in lieu of the classical Wagner's earth method. In this approach, the guard circuit and the detector, D, are maintained automatically, at the same potential, by means of a unit gain operational amplifier, whereby only a single balance step is required for the bridge. This feature, together with other improvements in the Schering bridge, is well exemplified in the Tettex precision Schering bridge, which has been designed for use on thin dielectric specimens up to 2 kV; its circuit is depicted in Fig. 10.

The bridge is limited in voltage, since now the lower arms are capacitive in nature, in order to attain a higher sensitivity as the stray capacitances are thus greatly reduced. The capacitance of the specimen, C, is obtained by an adjustment of C_4 to yield

$$C = \frac{C_s C_3}{C_4} \tag{40}$$

and the value of tan δ at the null is obtained by adjustment of R_3; the already low dielectric loss standard capacitor, C_s, is

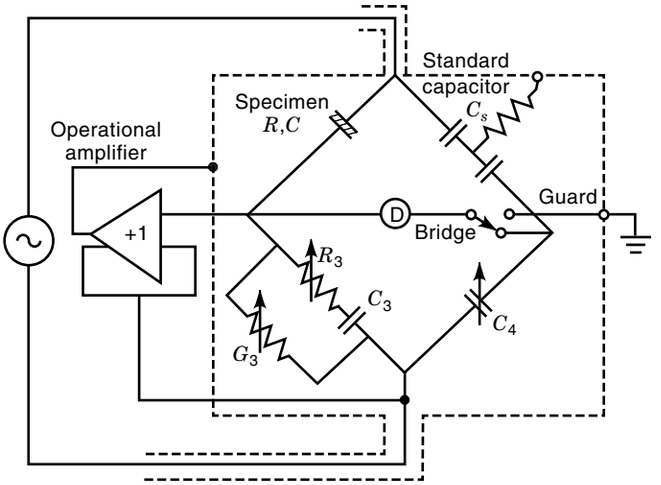

Figure 10. Schematic diagram of precision Tettex Schering bridge for measurements at power frequency (21).

artificially reduced to zero, such that the tan δ value of the specimen becomes

$$\tan\delta = \omega R_3 C_3 + \frac{G_3}{\omega C_3} \tag{41}$$

In the measurements carried out with Schering bridges, the capacitance and tan δ values of the dielectric specimens are obtained in terms of the resistance and capacitance elements of the bridge. Hence, the precision and accuracy of the measurements are determined by the accuracy of these resistances and capacitances themselves. Precise dielectric measurements may also be performed by means of an inductively coupled voltage divider, utilizing a transformer arrangement, thereby circumventing some of the accuracy and stability constraints associated with resistive and capacitive elements (2,22). Perhaps one of the finest precision/accuracy commercially available transformer ratio arm bridges for variable frequency measurements in the range from 10 Hz to 100 kHz, is that of Gen Rad, under the designation Type 1621 transformer ratio arm bridge. Its schematic circuit diagram is delineated in Fig. 11. A twelve-digit readout of the specimen capacitance C_x with a 10-ppm accuracy is provided within the range of 10^{-7} pF to 10 μF. A basic accuracy of 0.1% is attainable for conductance, G_x, measurements within the range of 10^{-10} to 10^3 μS—that is, a tan δ value of 10^{-7} at 1 kHz may be determined with a four-figure resolution.

The capacitances C_A and C_B shunting the transformer winding and the specimen, respectively, do not introduce any error into the measurement, since the former produces only a reduction of the voltage across the specimen, while the latter causes only a decrease in the sensitivity of the detector, D. In balancing the bridge, the multiple tapped transformer principle is utilized in the course of the resistive and capacitive decade adjustments. Accordingly, the balance equation at the null of the bridge is given by

$$\begin{aligned} N_2(G_x + j\omega C_x) = N_1[&(\beta_1 G_1 + \beta_2 G_2 + \cdots + \beta_n G_n) \\ &+ j\omega(\alpha_1 C_1 + \alpha_2 C_2 + \cdots + \alpha_n C_n)] \end{aligned} \tag{42}$$

Equating the real and imaginary terms yields the capacitance of the specimen

$$C_x = \frac{N_1}{N_2}[\alpha_1 C_1 + \alpha_2 C_2 + \cdots + \alpha_n C_n] \tag{43}$$

and the conductance

$$G_x = \frac{N_1}{N_2}[\beta_1 G_1 + \beta_2 G_2 + \cdots + \beta_n G_n] \tag{44}$$

The dissipation factor of the specimen as a function of frequency is obtained as

$$\begin{aligned} \tan\delta &= \frac{G_x}{\omega C_x} \\ &= \frac{[\beta_1 G_1 + \beta_2 G_2 + \cdots + \beta_n G_n]}{\omega[\alpha_1 C_1 + \alpha_2 C_2 + \cdots \alpha_n C_n]} \end{aligned} \tag{45}$$

Note that the transformer ratio arm bridge views the dielectric specimen as an RC parallel equivalent circuit.

A computer-controlled automatic transformer ratio arm has been developed for measurements at power frequencies under high-voltage conditions (24). The bridge circuit is delineated schematically in Fig. 12, in which the coarse and fine balances are obtained by variation of the current comparator windings N_1, N_2 and N_3, N_4, respectively. The currents in N_3 and N_4 are controlled by the multiplying analog-to-digital converters (ADCs), α and β, respectively, and are proportional to the current in the standard high-voltage capacitor, C_s. The ampere turns equation for the balance condition at an applied voltage V across the specimen when the current, I, is equal to zero in the winding of the null detector, N_1, is given by

$$V(G_x + j\omega C_x)N_1 = j\omega C_s V(N_2 + \alpha R G_1 N_4 - j\beta R G_2 N_3) \tag{46}$$

Equating the real and imaginary terms leads to the approximate expressions for the parallel, equivalent capacitance, C_x, and dissipation factor, tan δ of the dielectric (18,24):

$$C_x = \frac{(N_2 + \alpha)C_s}{N_1} \tag{47}$$

and

$$\tan\delta = \frac{\beta R G_2}{1 + \dfrac{\alpha}{N_2}} \tag{48}$$

The automation of the power frequency transformer ratio arm bridge results in a reduction of the accuracy of the tan δ measurement from $\pm 1 \times 10^{-7}$ to $\pm\ 1 \times 10^{-5}$.

Radio Frequency Methods (1–200 MHz)

Bridge techniques become unsuitable for measurements at frequencies beyond 1 MHz, because of the onset of inductance effects and, as a consequence, within the radio frequency region of 1 MHz to 200 MHz, resonance rise (Q meter) or susceptance variation methods must be employed (2,18). Within these frequencies, three-terminal techniques become inapplicable and measurements must be carried out using two-terminal specimen holders.

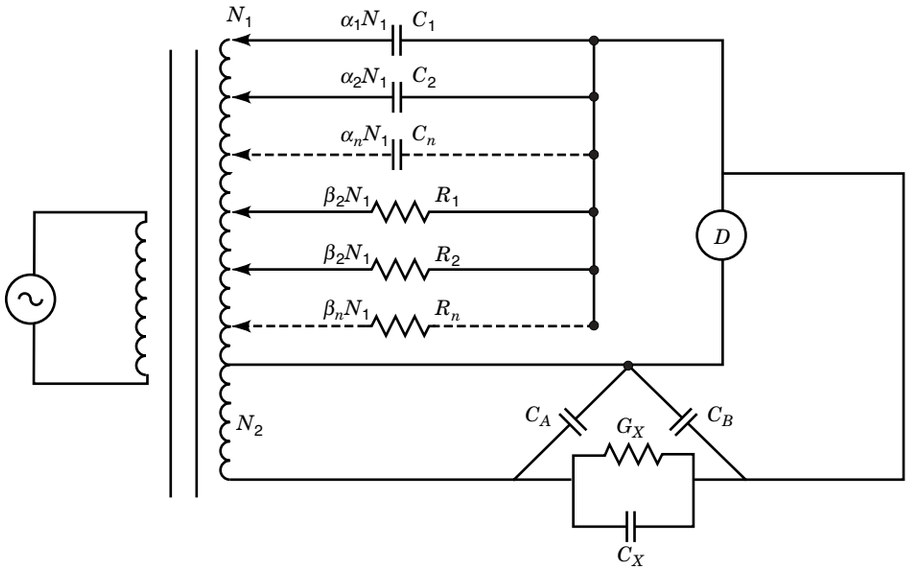

Figure 11. Basic circuit of Gen Rad Type 1621 precision transformer ratio arm bridge (23).

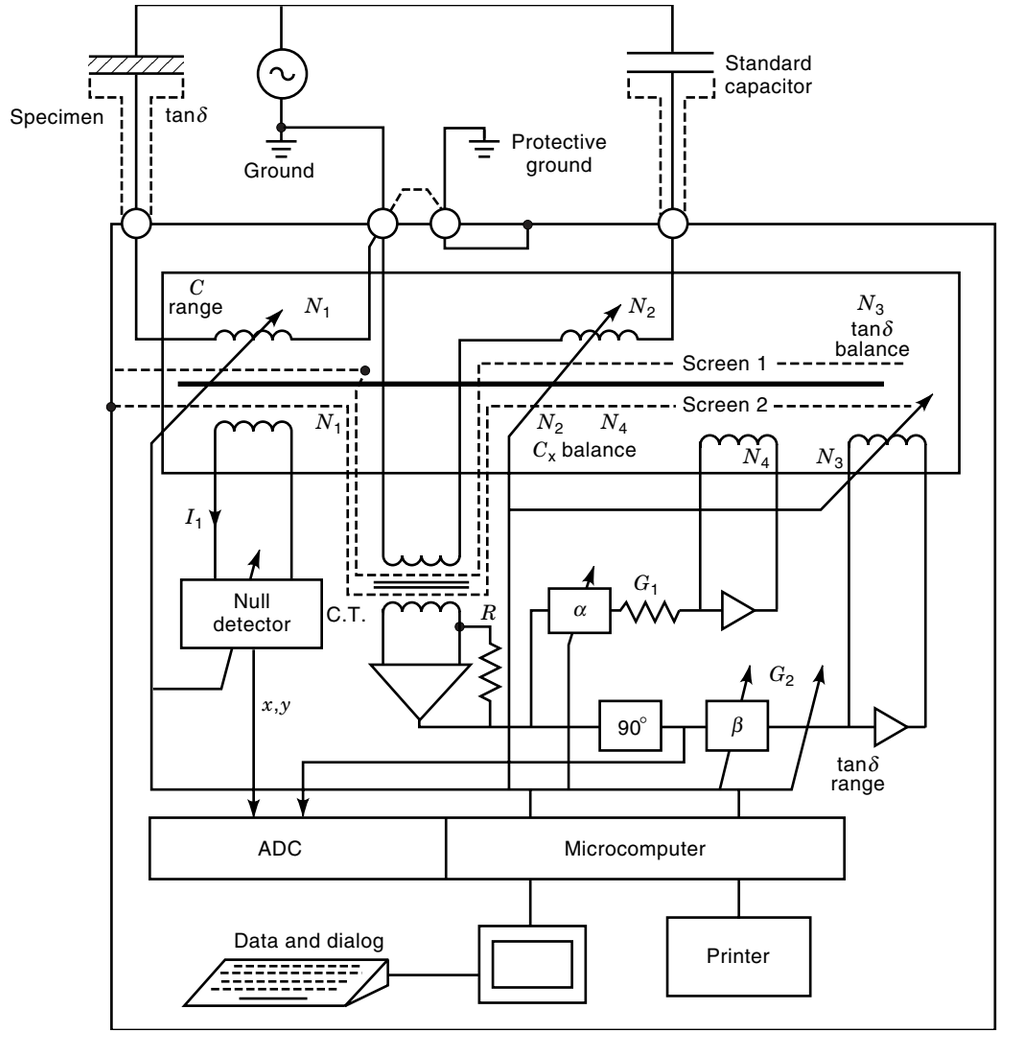

Figure 12. Automated power frequency transformer ratio arm bridge with computer control for measurements at high voltages (24).

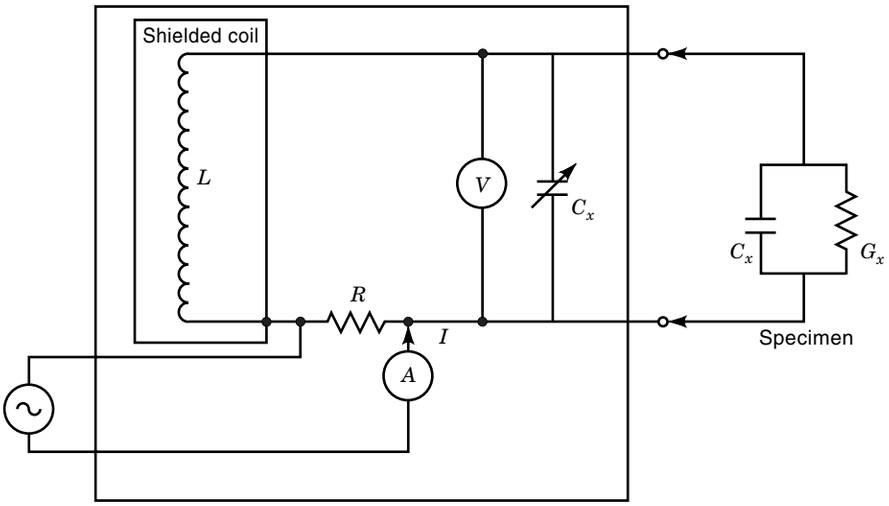

Figure 13. Q-meter circuit.

The basic Q-meter circuit is shown in Fig. 13, in which the capacitance and tan δ values of the specimen are determined in terms of a variable standard capacitor, C_s and the quality factor, Q, of the circuit. The coil, L, denotes a range of shielded fixed-inductance coils that are employed to establish resonance of the circuit with the specimen (G_x, C_x) inserted and removed. By definition, the Q value of the circuit is equal to the ratio of the peak voltage, V_o, across the oscillator to that across the inductance, V_L, such that

$$\begin{aligned}\frac{V_o}{V_L} &= \left(1+\frac{\omega^2 L^2}{R^2}\right)^{1/2} \\ &= (1+Q) \\ &\simeq Q\end{aligned} \tag{49}$$

for $Q \gg 1$. The voltmeter (V) of the Q-meter is calibrated to read the Q values directly, since Q is given by V/IR. Representing the values of C_s', Q' and C_s, Q as those obtained with the specimen disconnected and connected, respectively, yields the capacitance C_x and tan δ values of the specimen as

$$C_x = C_s' - C_s \tag{50}$$

and

$$\tan\delta = \frac{1}{Q_x} \tag{51}$$

where

$$Q_x = [(C_s' - C_s)/C_s'][Q'Q/(Q' - Q)] \tag{52}$$

When the measurements are carried out at high frequencies, a stiff short copper connecting wire should be employed between the specimen and the high-potential terminal of the Q-meter, so that when disconnected, its same geometrical position, and configuration, a short distance removed from the high-potential terminal, may be maintained, to ensure negligible change in the stray effects of the two positions of the connecting wire. With parallel-plane micrometer electrode specimen holders, accuracies of ±(0.1% + 0.02 pF) and ±(2% + 0.00005 pF), for the respective capacitance and tan δ values of solid dielectric specimens may be achieved (16). For solid specimens, an excellent precision reproducibility of ±0.05% and $\pm 5 \times 10^{-5}$ for C_x and tan δ, respectively, may be obtained by means of liquid displacement type specimen holders (25). A fluid displacement cell for use at 1 MHz, consisting of a fixed-plate, two-terminal, self-shielding capacitor, in which the edge and ground effects are taken into account, is depicted in Fig. 14.

The cell is most frequently employed for measurements at 1 MHz on polyethylene, though cell designs for frequencies up to 100 MHz are available. The fluid which is used in conjunction with polyethylene specimens is silicone with a kinematic viscosity of 1.0 cSt (1×10^{-6} m^2/s) at 23°C, whose dielectric constant matches that of polyethylene, and whose tan δ value between 100 kHz and 1 MHz is negligibly small (about 5×10^{-5}). The separation between the fixed measuring electrodes of the cell design in Fig. 14 is 1.52 ± 0.05 mm, thereby restricting the specimen thickness to 1.27 mm, in order to allow for the formation of a finite liquid film thickness on both sides of the solid dielectric

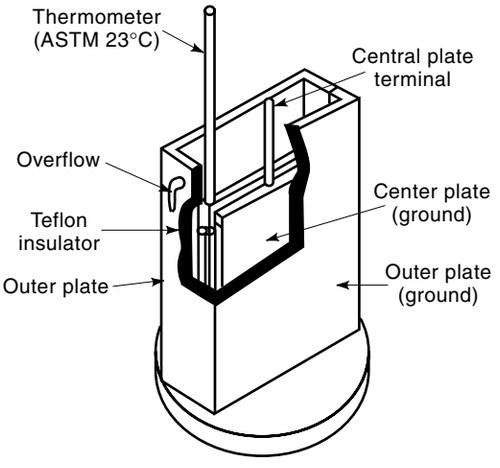

Figure 14. Fluid displacement cell with a fixed electrode separation equal to 1.52 ± 0.05 mm after ASTM Test Standard D1531 (25).

specimen adjacent to the central (high-potential) and outer (ground potential) plate electrodes or terminals. Two identical sizes (68.3 × 100 mm) of polyethylene sheet or slab specimens are employed, and measurements are made on the specimens inserted in the silicone fluid and then on the silicone fluid itself with the specimens removed.

The real value of the permittivity or dielectric constant of the polyethylene specimen, ϵ', is obtained from the relation

$$(\epsilon' - \epsilon'_\ell) = \frac{\Delta C}{C_0}\left(\frac{d_0}{d}\right) \tag{53}$$

where ϵ'_ℓ is the real value of the permittivity of the silicone fluid at the measurement temperature, d_0 denotes the electrode separation, d represents the average thickness of the two specimens, and C_0 is the capacitance in vacuo of the double-plated capacitor within the fluid displacement cell, given by

$$C_0 = 2\left[\frac{\epsilon_0 A}{d_0}\right] \tag{54}$$

where ϵ_0 is the permittivity of free space, A is the area of the center capacitor plate or electrode; the value of ΔC is obtained from

$$\Delta C = (C_2 - C_1) \tag{55}$$

where C_2 is the measured capacitance with the two solid dielectric specimens immersed in the silicone fluid and C_1 the corresponding value with the two specimens removed.

The dissipation factor, tan δ, of the two polyethylene specimens is defined by

$$\tan \delta = \tan \delta_\ell + (\tan \delta_c - \tan \delta_\ell)[d_0/d] \tag{56}$$

where tan δ_ℓ is the dissipation factor of the silicone fluid itself and is given by

$$\tan \delta_\ell = C_T(Q_c - Q_1)/C_\ell Q_0 Q_1 \tag{57}$$

where C_T represents the total capacitance of the tuned Q-meter resonant circuit prior to the connection of the specimen cell, Q_0 denotes the quality factor of the circuit at resonance prior to the connection of the ungrounded lead to the cell terminal, and Q_1 is the quality factor of the measuring circuit at resonance following the connection of the lead to the terminal of the cell containing the silicone fluid only, and C_ℓ is the capacitance of the silicone fluid determined from the relation

$$C_\ell = (C'_1 - C_1) \tag{58}$$

where C'_1 is equal to the capacitance reading following the connection of the leads to the circuit terminals before the connection of the ungrounded lead to the cell terminal. The value of the dissipation factor, tan δ_c, obtained with the polyethylene specimens immersed in the cell, is determined from

$$\tan \delta_c = C_T(Q_0 - Q_2)/(\epsilon'_\ell C_0 + \Delta Q)Q_0 Q_2 \tag{59}$$

where Q_2 is the quality factor with the two solid specimens inserted in the cell.

The susceptance variation method originally propounded by Hartshorn and Ward (26) with subsequent refinements (27,28) is perhaps the most common method utilized for permittivity and loss measurements over the frequency region extending from 100 kHz to 200 MHz. The technique is based on the half-power point measurements of voltage across an LC resonant circuit, with the solid or liquid specimen inserted and removed from the test cell. A modified susceptance variation circuit and a cross-sectional profile view of the associated micrometer adjustable holder for solid specimens are depicted in Figs. 15 and 16, respectively. For liquids, the specimen holder is similar to that depicted in Fig. 16, except that two parallel concave electrodes are employed to permit containment of the liquid specimen.

The micrometer adjustable electrode system depicted in Fig. 16 portrays a solid dielectric specimen between plane-parallel electrodes. In the measurement procedure, resonance is first established with the specimen inserted between the electrodes and the maximum value of the voltage, e_1, of the ac to dc converter is recorded. Thereafter, the specimen is removed and the separation of the electrodes is reduced until resonance is reestablished; this resonance point is characterized by a larger output voltage, e_o, of the ac to dc converter. The capacitance of this air gap spacing is numerically equal to the capacitance of the specimen, C_x, and is obtained directly from the calibrated reading of the main micrometer setting. Manipulation of the main micrometer head, in conjunction with the small vernier or incremental capacitor, yields the half-power points of the resonance curve; the resulting width of the resonance curve is equivalent to a capacitance change, designated as ΔC_0. It is the square law detection feature of the instrument that relates the ΔC_0 value directly to the recorded

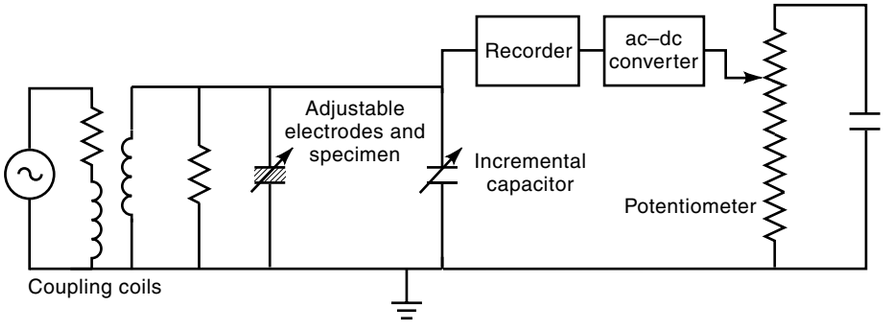

Figure 15. Schematic circuit diagram of modified Hartshorn and Ward susceptance variation circuit (27).

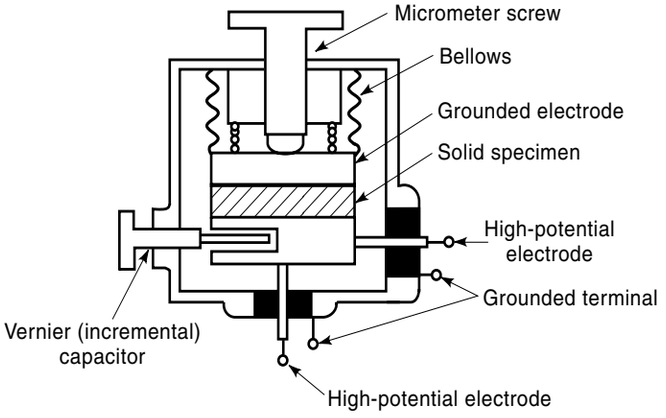

Figure 16. Micrometer adjustable electrode for use in conjunction with the susceptance variation circuit (26).

change of reading in the incremental capacitor. Hence the dissipation factor of the specimen (27) is given by

$$\tan \delta = [(e_o/e_1)^{1/2} - 1] \frac{\Delta C_0}{2C_x} \tag{60}$$

The real value of the permittivity, ϵ_r', is normally obtained in terms of the thickness of the specimen, d_s, and the quantity, Δd

$$\epsilon_r' = \frac{d_s}{d_s - \Delta d} \tag{61}$$

where Δd represents the decrease in separation of the main electrodes in air required to restore the same capacitance as that obtained with the specimen placed between the electrodes. An accuracy of 1% is achievable on permittivity measurements and tan δ may be determined to within $\pm 1.0 \times 10^{-6}$.

PERMITTIVITY AND LOSS MEASUREMENTS ON DISTRIBUTED PARAMETER SPECIMENS

Dielectric specimens behave as distributed parameter systems when the wavelength of the electromagnetic field becomes comparable to or is less than the physical dimensions of the specimen. The transition from lumped to distributed parameter behavior occurs generally within the frequency range from 300 MHz to 600 MHz. The high-frequency dielectric measurements represent a vast area of endeavor, which involves the use of resonant cavities of cylindrical and rectangular shapes, waveguides, or transmission lines, including quasi-optical procedures, as well as optical methods requiring the use of spectrometers and interferometers. Since it would not be feasible within the space constrains to cover, even in a cursory manner, all test method variations over the millimeter and submillimeter wavelengths, the test procedures followed over this range of frequencies will be illustrated by a number of widely used and representative test methods.

Reentrant Cavity Method (300 to 600 MHz)

The reentrant cavity measurement technique constitutes, in essence, an extension of the Hartshorn and Ward method; it uses the same specimen cell arrangement, with the exception that the inner walls are silver plated, and the oscillator signal is admitted into the cell cavity via a coupling loop with a detector loop situated on the opposite wall of the concentric coaxial cell cavity (29). The reentrant cavity is calibrated as a wavemeter, with the main micrometer adjustable specimen capacitor acting as the prime frequency control device and the vernier capacitor as an incremental control device (refer to Fig. 16). As in the case of the Hartshorn and Ward technique, the dielectric parameters are determined in terms of the width of the resonance curve with the specimen inserted between the measurement electrodes and then removed.

Coaxial Line-Waveguide Methods (500 MHz to 50 GHz)

Waveguide or transmission line methods are based on the shorted coaxial line technique developed by Roberts and von Hippel (30). Although for low loss dielectric solids and liquids, the technique yields optimum performances for microwave frequencies up to 50 GHz; the method has been used up to 95 GHz (31).The confinement of the electrical field within the hollow waveguide's circular or rectangular geometry eliminates stray capacitance and inductance effects. A standing wave pattern results within the waveguide, from a reflection of the incident wave at the short-circuit termination adjacent to where the solid specimen is inserted as depicted in Fig. 17. When liquid specimens are tested, the waveguide is mounted in a vertical position (18). Figure 17 indicates the position of the electrical nodes (position of the interference minima), with the width of the nodes, Δx, as indicated at the 3-dB points. In terms of Δx, the voltage standing wave ratio, abbreviated as VSWR, or r, may be expressed as

$$r = \lambda_{gs}/\pi \Delta x \tag{62}$$

where λ_{gs} is the wavelength of the slotted coaxial line; it is along the slot that a traveling probe is displaced to determine the VSWR. Since the value of Δx changes when the specimen is removed from the waveguide, the VSWR, r, also changes accordingly.

Perhaps one of the most common shorted coaxial transmission line arrangements in use is that described in ASTM D2520 (32), which is suitable for temperature-controlled measurements up to 1650°C, when utilized in conjunction with a platinum alloy with 20% rhodium as the material for the specimen holder; its schematic diagram is delineated in Fig. 18. A micrometer head in the slotted waveguide section is capable of measuring node width distances to within ± 0.0025 mm. The traveling probe has an adjustable depth control and the detector is of the square law type that constitutes a re-

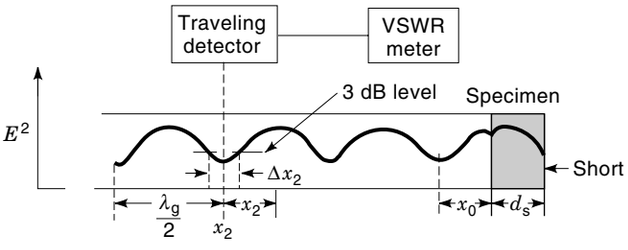

Figure 17. Standing voltage wave pattern in a shorted coaxial waveguide containing a solid dielectric specimen (2).

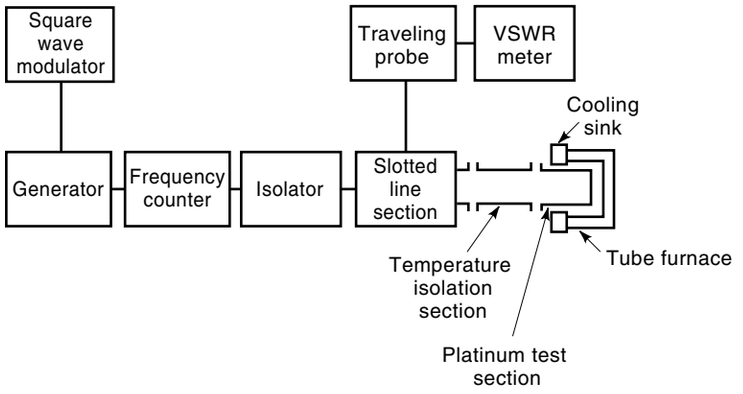

Figure 18. Schematic diagram of shorted rectangular waveguide with a temperature controlled test specimen section (after ASTM D2520) (32).

quirement for the VSMR meter. The setting of the isolator is fixed at 30 dB, and the square wave modulator provides a constant frequency of 1 kHz; the isolator or attenuation pad prevents frequency pulling between the generator and the remainder of the circuit. The lateral dimensions of the solid specimen are selected to be 0.05 ± 0.025 mm less than those of the transmission line. The rectangular waveguide is operated in the fundamental TE_{10} mode, which is analogous to the TEM mode of a cylindrical waveguide, in which the electrical field is radial and the magnetic field concentric with the coaxial geometry. The cut-off wavelength, λ_c, in the TE_{10} mode is equal to $2a$—that is, twice the width a of the rectangular guide. Thus, the wavelength with an empty holder at the required test temperature is given by

$$\begin{aligned}\lambda_{gh}^{-2} &= \lambda_0^{-2} - \lambda_c^{-2} \\ &= \lambda_0^{-2} - (2a)^{-2}\end{aligned} \tag{63}$$

where λ_0 is the wavelength of the radiation in free space and is equal to c/f, where c is the velocity in free space and f is the frequency.

With the specimen of thickness d_s inserted adjacent to the short in the waveguide, the impedance of the line at the specimen–air interface (33) is given by

$$Z_{\text{in}} = (j\omega\mu_0/\gamma_2)\tanh(\gamma_2 d_s) \tag{64}$$

where μ_0 is the permeability of the nonmagnetic dielectric material, which is identical to that in free space. Assuming negligible losses in the walls of the waveguide, the propagation constant of the coaxial waveguide, γ_2, containing the specimen is given by

$$\gamma_2 = 2\pi(\lambda_c^{-2} - \epsilon_r'\lambda_0^{-2})^{1/2} \tag{65}$$

The load impedance at a phase distance φ from the observed electrical node for the value of the VSWR, r, given by Eq. (62) (34) is

$$Z_{\text{meas}} = f\mu_0\lambda_g[(1 - jr\tan\varphi)/(r - j\tan\varphi)] \tag{66}$$

where λ_g is the wavelength of the guide and is equal to $2\pi/\beta_2$; here β_2 is the phase coefficient of the waveguide with the specimen inserted; φ is the corrected phase distance, defined by

$$\varphi = 2\pi[(N/2) - (d_s/\lambda_{gh}) \pm (x_2 - x_1)\lambda_{gs}] \tag{67}$$

where N represents the smallest integer for which φ is positive, x_2 is the position of the traveling detector with the specimen inserted, as indicated in Fig. 17, and x_1 is the equivalent distance with the specimen removed.

Equating the impedances Z_{in} and Z_{meas} yields

$$\frac{\tanh\lambda_2 d_s}{\gamma_2} = \frac{\lambda_{gh}(1 - jr\tan\varphi)}{2\pi j(r - j\tan\varphi)} \tag{68}$$

Equating the real and imaginary terms yields the relative real value of the permittivity, ϵ_r', of the specimen as

$$\epsilon_r' = [(\beta_2/2\pi)^2 + \lambda_c^{-2}]/\lambda_0^{-2} \tag{69}$$

and, for low-loss specimens (34), the dissipation factor simplifies to

$$\tan\delta = \frac{\Delta x(1 - \lambda_0^2/\epsilon_r'\lambda_c^2)(1 + \tan^2\varphi)}{d_s\{[1 + \tan^2\beta_2 d_s] - [(\tan\beta_2 d_s)/\beta_2 d_s)\}} \tag{70}$$

where the width of the node, Δx, that would be measured at the face of the specimen is given by

$$\Delta x = \Delta x_2 - \Delta x_1 \tag{71}$$

The principal factors affecting the accuracy of the measurements are associated with the assumption that losses at the walls of the waveguide are negligible and that the finite air-gap between the solid specimen and the walls of the waveguide does not influence appreciably the results; evidently, the latter error does not arise with liquid specimens (18). However, accuracies of ±1% for ϵ_r' and ±200 radians for the loss angle δ are achievable.

Resonant Cavity Methods (about 500 MHz to 60 GHz)

A resonating cavity may be viewed as a transmission line, which is shorted at both ends that are separated by an arbitrary multiple of one-half the operating wavelength. The insertion of a dielectric specimen into the cavity alters the wavelength and, as a consequence, the change in the quality factor, Q, of the cavity with the specimen inserted and removed can be used to derive the dielectric parameters of the specimen. Since resonant cavities have intrinsically high values of Q, they constitute an effective means for measuring low-loss dielectric materials. The specimens may have different geometrical configurations such as spheres, sheets, disks,

rods, and so forth, and may fill the cross-section of the beam, if necessary. The required specimen size becomes smaller as the cavity size diminishes with frequency, thereby also necessitating a redesign of the cavity with each octave increase in frequency. For frequencies above 60 MHz, the reduced cavity sizes, irrespective of their shape, rapidly approach a practical limit. Although open resonant cavities or interferometers may exceed substantially the frequency of 60 MHz (35), their applicability is confined to specimens having dielectric constants in excess of 5.

A coaxial waveguide shorted at one end becomes a resonant cavity when shorted at both ends. It may be resonated either by varying the frequency of the externally applied field or by varying the radial or axial dimensions of the cavity itself. A very widely used rectangular microwave cavity design for operation in the transverse electric field, TE_{1ON} mode, is depicted in Fig. 19. Note that, in the mode designation code, the first subscript denotes the number of half-waves across the shorted waveguide, the second subscript refers to the number of half-waves from top to bottom of the waveguide, and the third subscript represents the odd number of half-waves along the waveguide. The closed cavity arrangement in Fig. 19 is identical to that given in the test method described in ASTM D2520 (32). It is of paramount importance that the diameter of the iris holes in the transmitting and detecting ends be small to achieve high Q values. The particular design of the shown resonant cavity is intended for use with solid rod-shaped specimens, which are held suspended between the top and bottom holes that are drilled into the waveguide (refer to Fig. 19). The resonant frequency of the specimen is defined by

$$f_0 = 15[(1/w)^2 + (N/d)^2]^{1/2} \tag{72}$$

where d is the physical length of the closed cavity and w its width (both in cm), N denotes the odd number of half-waves along the cavity, and the resonant frequency is in GHz. It is palpably evident, from Eq. (72), that higher test frequencies require closed cavities with increasingly reduced physical dimensions.

The measurements may be carried out either by means of the traditional VSWR meter utilizing a point-by-point approach or, for more rapidly obtainable results, a frequency sweep generator may be employed, as portrayed in the schematic test circuit of Fig. 20, in accordance with an IEC method (36). The latter method may be computerized, in order to minimize errors, by recording simultaneously dual outputs from the signal generator and the cavity.

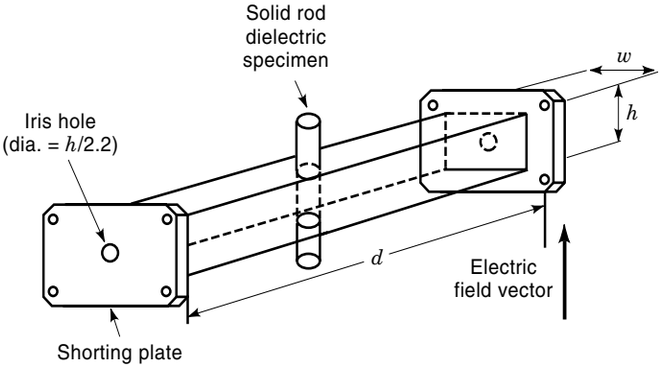

Figure 19. Closed rectangular resonant cavity for tests on solid rod-shaped dielectric specimens (after ASTM D2520) (32).

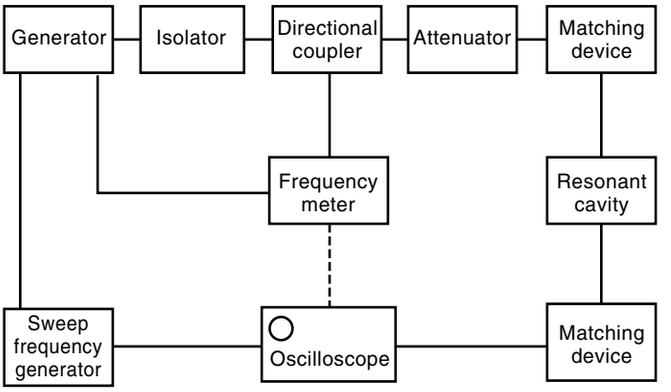

Figure 20. Microwave closed resonant cavity measurement system, using a sweep frequency generator technique (after IEC Publ. 377-2) (36).

The measurements are carried out with the empty cavity and then with the specimen inserted. The quality factor, Q_0, of the empty cavity is given by

$$Q_0 = \frac{f_0}{\Delta f_0} \tag{73}$$

where the half-power bandwidth of the empty resonant cavity is

$$\Delta f_0 = f_{02} - f_{01} \tag{74}$$

and f_{01} and f_{02} are the lower and upper frequency half-power (3 dB) points; the 3 dB points are established by means of a variable precision attenuator. When the specimen is inserted into the cavity, the quality factor, Q_s, becomes

$$Q_s = \frac{f_s}{\Delta f_s} \tag{75}$$

where f_s is the new resonant frequency of the closed cavity containing the specimen and the half power bandwidth is

$$\Delta f_s = f_{s2} - f_{s1} \tag{76}$$

where f_{s2} and f_{s1} are respectively, the upper and lower 3 dB point frequencies. The value of the relative real permittivity, ϵ_r', and the dissipation factor, tan δ, may now be determined from

$$\epsilon_r' = \left[\left(\frac{V_0(f_0 - f_s)}{2V_s f_s}\right) + 1\right] \tag{77}$$

and

$$\tan\delta = \frac{\left[\frac{V_0}{4V_s}\left(\frac{1}{Q_s} - \frac{1}{Q_0}\right)\right]}{\left[\left\{\frac{V_0(f_0 - f_s)}{2V_s f_s}\right\} + 1\right]} \tag{78}$$

where V_s and V_0 are respectively, the volumes of the specimen and the empty cavity. Note that the measured quantities are not contingent upon the dimensions of the closed cavity. An accuracy to within 0.5% for the permittivity and approximately 5% for the dissipation factor are attainable. The specimen size and location within the cavity plays an important role; these two parameters influence the magnitude of the difference between Q_s and Q_0 upon which the precision and accuracy depend. A high Q value for the cavity is thus important, since the 3 dB point frequencies become more clearly defined.

Quasi-Optical and Optical Methods (30 GHz to 3000 GHz)

Dielectric measurements at microwave frequencies in excess of 60 GHz become increasingly more arduous, as a result of the unduly small size of resonant cavity required. The difficulty is circumvented by employing for the microwave frequency range the same methods as those that are utilized in light wave optics; such procedures are commonly referred to as quasi-optical or free space techniques. In analogy to an optical spectrometer, the collimator in a quasi-optical microwave type instrument consists of a parabolic reflector connected to a microwave generator, with the plane wave source directed toward the dielectric specimen (37). The latter is in sheet form and is mounted upon an object table, as in the case of an optical spectrometer. Another parabolic reflector (substituting an optical telescope), connected to a detector, receives the signal which is either reflected from or transmitted through the sheet specimen. Thus, the resulting attenuation in the path between the transmitting and receiving parabolic reflectors constitutes a measure of the dielectric loss in the intervening dielectric sheet (38).

Quasi-optical techniques also include the use of optical cavity resonators, which are suitable for measurements within the millimeter and submillimeter wavelengths of the electromagnetic spectrum. This differs from the usual closed cavity microwave resonator, in that the length of the resonator corresponds to a length number of wavelengths, while the specimen (in sheet form) assumes only a small fraction of the overall length (2). There are three types of quasi-optical resonators, namely, the classical Fabry-Pérot interferometer, the confocal resonator, and the semiconfocal resonator. The confocal resonator has the advantage that the electrical field is more confined to the axis of the resonator, resulting in Q values generally higher than 10^5 and lower diffraction losses. The Q of a semiconfocal resonator is approximately equal to half that of the confocal resonator.

For illustrative purposes, the measurement procedure followed with a quasi-optical confocal resonator (39), delineated in Fig. 21, will be described, which has been successfully used at frequencies up to 343 GHz. As with any resonant cavity, the resonant frequency of the quasi-optical cavity is perturbed by the insertion of the specimen. The specimen is intentionally mounted at an angle, θ, to the vertical axis of the cavity, in order to eliminate standing wave phenomena. The angle permits the waves reflected from the air–dielectric interface to escape from the resonator. The resonance is restored by reducing the distance ℓ between the two mirrors by an amount equal to $\Delta\ell$. The real value of the index of refraction, n', of the specimen (39) is then given by

$$\begin{aligned} n' &= (\epsilon_r')^{1/2} \\ &= \left(1 + \frac{\Delta\ell}{d_s} - \frac{\varphi}{\beta_0 d_s}\right) \end{aligned} \tag{79}$$

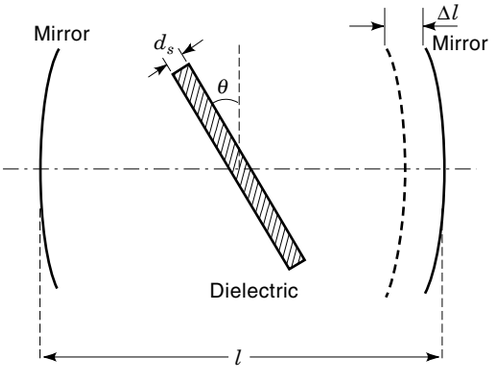

Figure 21. Quasi-optical confocal resonator arrangement (39).

where d_s is the thickness of the dielectric specimen, β_0 is the phase factor in free space and is equal to $2\pi/\lambda_o$, and the angle φ is defined by

$$\varphi = \tan^{-1}\left[\frac{\sin 2n'\beta_0 d_s}{\left(\dfrac{n'+1}{n'-1}\right) - \cos 2n'\beta_0 d_s}\right] \tag{80}$$

For tan δ measurements, the length of the empty quasi-optical confocal resonator must be adjusted to an odd number of half wavelengths at the resonant frequency for which the Q value is to be determined. The specimen must then be inserted at a position vertical to the axis of the resonator—that is, with $\theta = 0$, the Q value is maximized as the escape of the power from the resonator is minimized. With the resonant frequency restored as each mirror is moved inward a distance, $\Delta\ell/2$, the quality factor, Q_s, with the specimen inserted is then determined. The expression for the dissipation factor (39) follows as

$$\begin{aligned} \tan\delta = {} & \frac{\beta_0\ell - \beta(\Delta\ell + d_s)\left[1 + \dfrac{\sin\beta_0(\Delta\ell + d_s)}{\beta_0(\Delta\ell + d_s)}\right]}{Q_s\eta^2(\epsilon_r')^2\beta_s d_s\left[1 + \dfrac{\sin\beta_s d_s}{\beta_s d_s}\right]} \\ & + \frac{1}{Q_s} - \left\{\frac{Q_0\lambda_0/2\pi\ell}{\eta^2(\epsilon_r')^2\beta_s d_s\left[1 + \dfrac{\sin\beta_s d_s}{\beta_s d_s}\right]}\right\} \end{aligned} \tag{81}$$

where β_s is the phase constant in the dielectric medium and is equal to $2\pi/\lambda_s$; the value of η is

$$\eta = \left\{\frac{[(n')^2 + \omega t^2\beta_0 x_1]/(n')^2}{1 + \omega t^2\beta_0 x_1}\right\} \tag{82}$$

where x_1 denotes the distance from the reflector to the dielectric sheet.

In the frequency range from 300 GHz to 3000 GHz (wavelengths of 1 mm to 100 μm), true optical measurement techniques are employed. As this wavelength range overlaps the infrared region, infrared sources and detectors are utilized. If a broadband radiation source is employed, the component measurement frequencies, appearing at the

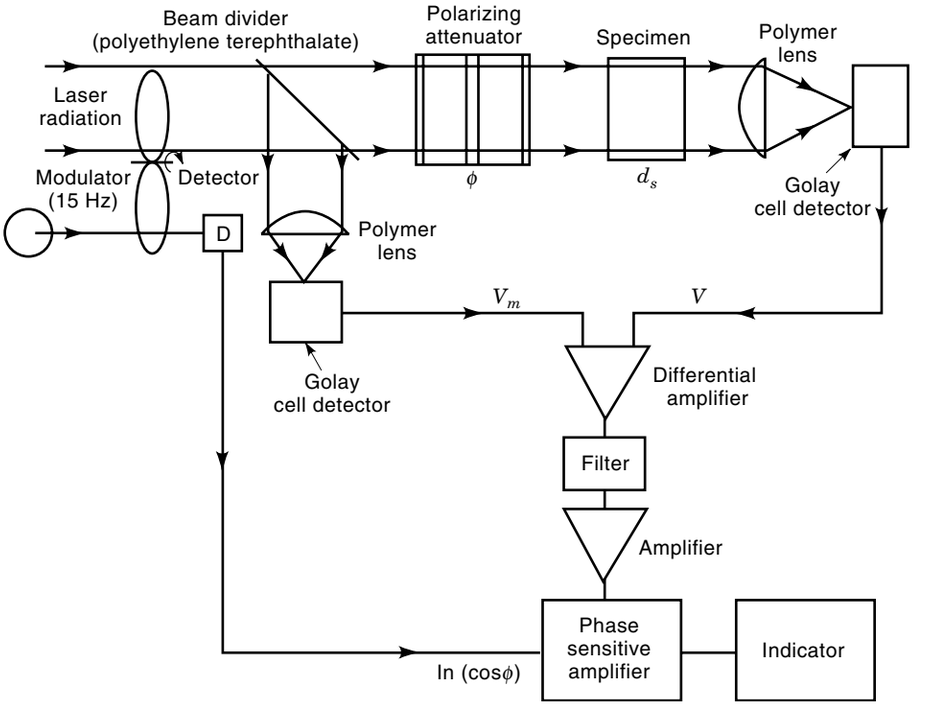

Figure 22. Dielectric absorption measurement system at optical frequencies with a laser radiation source (40).

output of an interferometer, are selected by means of a computer in terms of their Fourier components. Broadband radiation sources require more sensitive detectors; it is for this reason that laser sources, though monochromatic, appear to be more popular.

Figure 22 depicts an arrangement for the measurement of dielectric absorption at optical frequencies, utilizing a laser source (40). The attenuation of the transmitted signal is obtained by comparing the amplitude of the signal transmitted through the specimen, V, with a monitored incident signal, V_m. The method entails the use of different specimen thicknesses, d_s, which requires adjustment of the polarizing attenuator, in order to maintain a constant transmission loss.

The dissipation factor is related to the absorption coefficient, a_p, which is obtained from the relation (40)

$$\ell nA = a_p d_s + \text{constant} \tag{83}$$

the units of a_p are in nepers per cm; A is the reading of the attenuator, which is equal to $(\cos\varphi)^4$; here φ is the central polarizer angle of the attenuator. From the nature of Eq. (83), it is apparent that the absorption coefficient a_p can be obtained directly from a linear plot of ln$A$ versus the specimen thickness d_s. The imaginary part of the index of refraction is equal to $ca_p/4\pi f$, where f is the frequency. Hence, the relative real value of the permittivity is given by

$$\epsilon_r' = (n')^2 - \left(\frac{ca_p}{4\pi f}\right)^2 \tag{84}$$

and the relative imaginary value of the permittivity is

$$\epsilon_r'' = \frac{cn'a_p}{4\pi f} \tag{85}$$

The dissipation factor, which is equal to the ratio ϵ_r''/ϵ_r', is then

$$\tan\delta = \frac{8\pi f n' c a_p}{(4\pi f n')^2 - (ca_p)^2} \tag{86}$$

The foregoing approach is based on transmission techniques, but laser source reflection arrangements are also available. It should be observed that there are a number of variations in the types of interferometers available for dielectric measurements, including the classical Michelson interferometer, which, in conjunction with a broadband radiation source, is suitable for measurements up to 3000 GHz. Laser refraction measurements, based on the Mach–Zehnder approach, may also be employed to derive dielectric data. A comparison of the various optical measurement techniques at a large number of laboratories indicates that, whereas the real value of the index of refraction, n', may be determined to an accuracy of 1 percent, the errors in the measurement of the absorption coefficient, a_p, may be as high as 37% (41).

VOLTAGE BREAKDOWN STRENGTH MEASUREMENTS

Voltage breakdown strength measurements are carried out on insulating materials to determine whether these materials can withstand certain operating stresses without failure. Since voltage failure is frequently initiated at fault sites within solid insulating materials, the dielectric strength serves as an indicator of the homogeneity of the material. In liquid dielectrics, low dielectric strength values may be associated with moisture content, electrolytic contamination, and a high particle content. With gases for which the dielectric strength is a definite function of the composition of the gas (pure or mixture), dielectric strength data may be used to detect contamination from other gases, as well as determine the breakdown characteristics of intentionally combined gas mixtures.

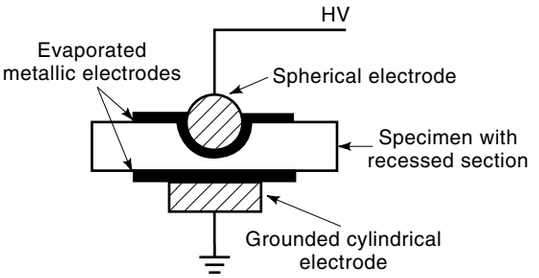

Figure 23. Spherical HV electrode with recessed solid specimen (42).

The dielectric strength of insulating materials is very much contingent upon the geometry of the test electrodes utilized. Sharp accentuated electrode edges lead to electrical field concentrations at the edges, which cause initiation of voltage breakdown of the material at voltages substantially below those that can be achieved under more uniform electrical field conditions. Thus voltage breakdown data are inextricably associated with the specific geometry of the test electrodes employed.

The true value of the breakdown strength or, more specifically, the intrinsic breakdown strength of the dielectric is obtained when the applied electrical field is perfectly uniform. A uniform field can be achieved by means of Rogowski–Rengier profile electrodes; however, the application of such recessed-type electrodes to solid specimens requires the embedding of the electrodes into the solid dielectric by means of a suitable molding process when plastic dielectrics specimens are tested. Several relatively simple recessed electrode systems have been developed, which do not entirely produce a uniform field, but which improve the electrical field configuration appreciably, thereby permitting the attainment of dielectric strengths approaching the intrinsic value. One such simplified arrangement is depicted in Fig. 23 (42).

The recess in the rigid solid dielectric may be machined to form a highly stressed region in the specimen, with the electrodes vapor deposited upon the dielectric to preclude any air gaps between the electrodes on the specimen. Alternatively, with nonporous solid dielectrics, conducting silver paint may be applied. Should spark-over occur at the edges prior to dielectric breakdown, the entire electrode assembly may be immersed in a mineral or silicone oil bath, provided the solid specimen is a nonporous material. The conductivity, σ_m, and dielectric constant, ϵ'_m, of the immersing medium must be selected, such that, under dc test voltages (43)

$$\sigma_m E_m > \sigma_s E_s \tag{87}$$

where E is the electrical field and the subscripts m and s refer, respectively, to the oil medium and the solid specimen. Under alternating test voltages,

$$\epsilon'_m E_m > \epsilon'_s E_s \tag{88}$$

If the liquid is partially conducting, then

$$\epsilon'_m E_m \sec \delta_m > \epsilon'_s E_s \sec \delta_s \tag{89}$$

where δ is the loss angle.

Although the intrinsic strength of a dielectric material provides information on the maximum breakdown strength attainable for that material and thus is used to ascertain the nature of the mechanism responsible for the breakdown, it is, per se, of little consequence in practice. In fact, the intrinsic breakdown strength is usually one to several orders of magnitude higher than the electrical breakdown stress obtained with regular parallel-plane electrodes, or with the various electrical insulation configurations existing in different electrical apparatus. For this reason, the type of electrodes used in standard routine breakdown tests on materials are relatively simple to use, and are designed to provide reproducible results primarily for comparison purposes.

Electrode Systems for Routine Breakdown Tests on Solid Specimens

Present practice in assessing the breakdown strength and the quality of solid, liquid, and gaseous dielectric materials for use in electrical apparatus and cables involves the use of a number of electrode systems, in accordance with national and international standards. For solid materials, the most commonly employed electrode system is the one-inch or 25 mm two-cylindrical electrode equal-diameter system portrayed in Fig. 24 (44). The edges of the electrodes are rounded to a radius of 3.2 mm, to minimize stress enhancement. In all dielectric strength tests, the thickness of the specimen must be specified, because the voltage stress, at which breakdown occurs, increases with a reduction of the specimen's thickness. That is, although very thin solid dielectric films may break down at low voltages, the corresponding breakdown stresses are appreciably higher than those for thick films of the same material, even though the latter may undergo breakdown at much higher applied voltages.

It is evident that equal-diameter electrodes systems must be concentric. This requirement may be circumvented by the use of two electrodes with different diameters, in accordance with IEC Publication 243, as depicted in Fig. 25 (45). Note that the IEC (International Electrotechnical Commission) standard specifies dielectric specimen thicknesses equal to or less than 3.0 ± 0.2 mm. If tapes of reduced width are tested, then rod electrodes of the geometry delineated in Fig. 26 are utilized. When breakdown tests are carried out on thin inorganic films with application to electron devices, miniature counter electrodes are vapor deposited onto the surface of the specimen. For the evaluation of embedding compounds or

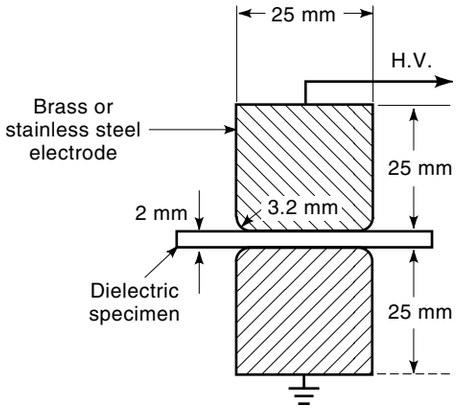

Figure 24. Equal-diameter electrode system for dielectric strength measurement on sheet materials (after ASTM D149) (44).

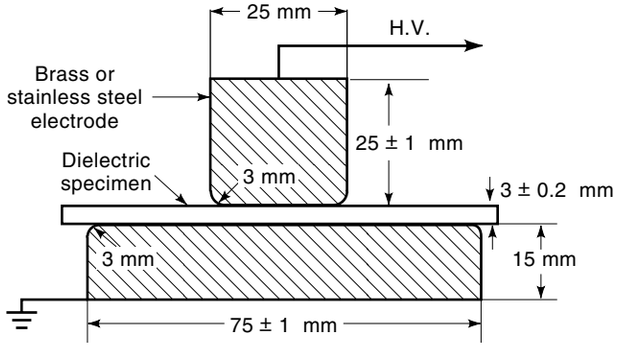

Figure 25. Unequal-diameter electrode system for dielectric strength measurements on sheet materials (after IEC Publication 243) (45).

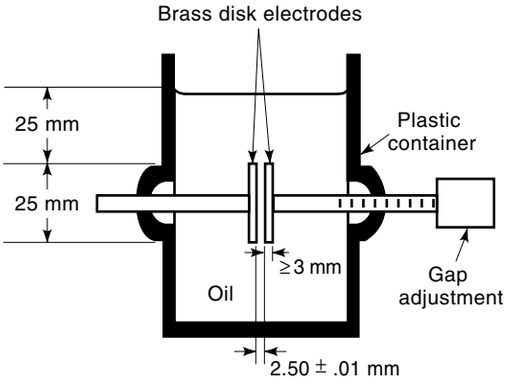

Figure 27. Parallel-plane square-edged electrode system for dielectric strength measurements on mineral oils (after ASTM D877) (46).

greases, the standard procedure of ASTM D149 requires hemispherical electrodes, having an equivalent diameter of 12.7 mm (44).

The foregoing described electrode systems for solid dielectric specimens are suitable for tests under ac power frequency, dc, and impulse conditions. The electrode systems, for routine determination of the dielectric strength of liquids, differ from those described for solids. Routine acceptance tests on oils of petroleum origin for electrical apparatus and cables are carried out with an oil cup containing parallel-plane polished brass electrodes, with an interelectrode spacing of 2.5 ± 0.01 mm. The electrodes have a diameter of 25 mm and a thickness of 3 mm; they are square at the edges and are separated from the inner wall of the oil test cup by a distance of not less than 13 mm. The oil test cup assembly is shown in Fig. 27 (46). The electrodes within the cell must be cleaned with a dry hydrocarbon solvent following each breakdown test; particular care must be taken to remove any carbonization deposits on the electrodes, and the electrodes must be repolished should any pitting of the surface manifest. Prior to admitting the liquid specimen into a cleaned test cell, the latter must be rinsed by the same liquid to remove any residues of the cleaning compound.

It is palpably evident from the geometrical configuration of the square-edge electrodes in Fig. 27, that electrical stress enhancement occurs at the edges of the electrodes and that, therefore, breakdown is likely to occur there. For lower viscosity dielectric liquids (<19 cSt or mm^2/s at 40°C), test electrodes, with the geometrical contour depicted in Fig. 28, have been found to be particularly effective in detecting decreases in the breakdown strength as a result of cellulose fiber contamination and absorbed moisture (47). These electrodes are normally referred to as the VDE (Verband Deutscher Electrotechniker) type electrodes. Measurements of dielectric strength are performed with electrode separations of either 1 or 2 mm, with a gentle downward oil flow at the electrodes created by means of a rotating impeller located beneath the electrodes in the test cell.

Since oil-filled and impregnated electrical power equipment is subjected to lightning and switching impulses, it is important to assess the quality of the oil in terms of its impulse breakdown strength. Under nonuniform electrical field conditions, the dielectric strength of the oil is contingent upon the polarity of the impulse in contradistinction to negligible differences observed under uniform fields. For this reason, nonuniform field electrode systems are frequently utilized for impulse tests. The electrodes may typically consist of either two 12.7 mm diameter brass or steel spheres or, for highly nonuniform fields, one such sphere and a steel needle point with a 0.06 mm radius of curvature at the needle tip (48).

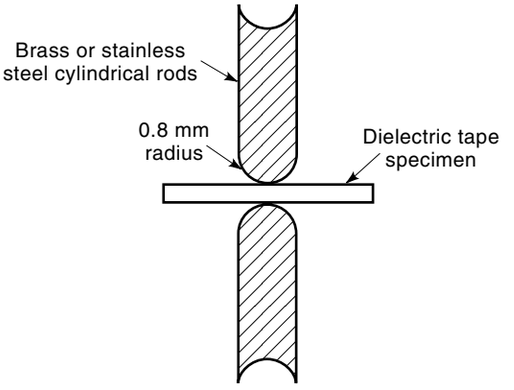

Figure 26. Cylindrical rod electrodes for dielectric strength measurements on thin narrow plastic tape or other narrow specimens (after ASTM D149) (44).

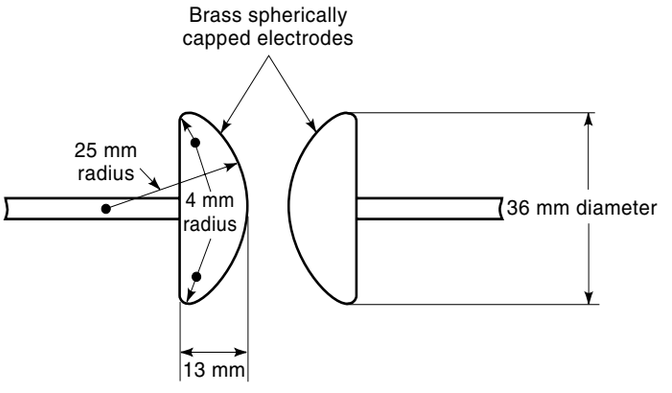

Figure 28. VDE electrode system for dielectric breakdown strength measurements on low-viscosity liquids (47).

The breakdown strength of gases is normally determined under quasi-uniform ac field conditions. Typical electrodes utilized for this purpose consist of a sphere-to-plane geometry, wherein the electrical field is uniform directly underneath the sphere adjacent to the plane, becoming increasingly less uniform as the separation between the sphere and the plane increases. With a sphere-to-plane geometry, electrical breakdown tends to always occur in the uniform field region—that is, at the point where the separation between the sphere and the plane is least. The high-potential sphere electrode may be of steel with a diameter of 0.75 inches or 19.1 mm, and the ground potential electrode may be a cylindrical brass plane with a 1.5 inch or 38.1 mm diameter (49). The tests are performed at 25°C at a standard pressure of 760 torr.

Voltage Breakdown Test Conditions and Procedures

The presence of lethal voltages in breakdown voltage tests necessitates strict adherence to high-voltage safety practices. Since the breakdown voltage may be a function of the ambient temperature, pressure, and humidity, depending upon where solid, liquid, or gas specimens are tested, these parameters should be recorded at the time of the test; solid insulating materials should be conditioned prior to the breakdown test, so that they may reach thermal and moisture equilibrium with the environment. For more lossy solid and liquid specimens, the application of intense alternating electrical fields may result in cumulative heat generation due to dielectric losses, thereby leading to a thermal instability induced breakdown. Solid specimens may contain gas cavity inclusions, within which intense recurring partial discharges at elevated alternating fields may cause rapid deterioration of the adjacent solid insulation, thus leading to conspicuously lower breakdown strengths. Both thermal and discharge mechanism associated breakdowns account for the lower observed ac breakdown strengths, as opposed to those measured under dc and impulse conditions. Where the breakdown strength is controlled by the thermal and partial discharge mechanism, the breakdown process is a strong function for the time of voltage application. Accordingly, the rate of voltage rise in any voltage breakdown test is an important parameter.

For solid dielectrics, the rate of ac sinusoidal voltage rise is fixed usually at 500 V/s, though more rapid or slower rise rates may also be used. Breakdown or rupture of the dielectric is indicated by an audible voltage collapse across the specimen, as well as a visual burn at the tip of the breakdown. In order to minimize stress-induced aging effects in the insulation undergoing the voltage breakdown test, ASTM D149 stipulates that the duration of a short-time breakdown must not exceed 20 s. In the past, a voltage step test was employed, whereby the voltage was raised in steps; at each step it was maintained for a preset time, prior to the next-step increment in voltage, until the ensuence of dielectric breakdown event—that is, an abrupt voltage collapse across the specimen. The use of the step procedure was required in the absence of voltage sources with automatically regulated rate of voltage-rise controls.

In dc dielectric breakdown strength determinations on dielectric material specimens, a single rate of voltage rise of 500 V/s is employed (50). Under direct voltages, the initial breakdown event produces a minute channel in the volume of the solid dielectric, whose trace is not readily discernible. Reapplication of the direct voltage results in successively lower breakdown voltages, which confirm that a dc breakdown has already occurred. Also, the additional damage and burning produced within the breakdown channel renders it more visible.

Impulse tests on solid dielectric specimens are performed by increasing the peak voltage of the impulse gradually, from an initial peak value of 0.7 times the anticipated breakdown voltage (45,50). The lightning impulse is simulated with an impulse waveform having a time to peak of 1.2 μs and a decay time of 50 μs to 50% of its initial peak value. Impulse breakdown is indicated by a voltage collapse at any point of the impulse waveform (2); the peak voltage value of this impulse wave is considered as the impulse breakdown voltage. Location of the actual breakdown channel caused by an impulse may require, as in the dc case, several reapplications of the voltage pulse, to cause additional carbonization within the breakdown channel.

In the measurement of dielectric strength of liquid specimens at ac power frequencies using the parallel-plane square-edge electrodes, a fixed voltage rise of 3 kV/s is generally specified (46). To avoid pitting of the test electrode surfaces, the short-circuit current at breakdown in the specimen is not permitted to exceed 10 mA/kV. For tests with the same electrode system under direct voltages, the same rate of voltage rise should be adequate. When the VDE-type electrodes are employed for low-viscosity liquids at power frequency, a much lower rate of voltage rise of 0.5 kV/s is preferred. Impulse breakdown tests performed on dielectric liquids are often carried out with both the simulated lightning impulse of the 1.2 by 50 μs form and a switching surge impulse form with a 100 μs rise time to peak and a decay time > 1000 μs. The impulse breakdown tests are carried out either at positive or negative polarities; often the measurements may be performed at both polarities. The measurement sequence at either polarity is begun at a voltage substantially below the expected impulse voltage breakdown level. Normally, three impulse waves are applied at each selected impulse voltage test level; it is an accepted practice to traverse at least three test levels prior to breakdown, with a fixed minimum time interval between each voltage level test. ASTM D3300 recommends a time interval of 30 s. The peak impulse voltage at breakdown is measured oscillographically across a calibrated resistive voltage divider. Whenever needle electrodes are employed, the geometry of the needle tip is altered, due to the energy released by the breakdown spark; this necessitates a change of the needle electrodes after each breakdown event.

Routine voltage breakdown strength measurements on insulating gases are normally performed under ac power frequencies, using a standard rate of voltage rise of 500 V/s (49). The breakdown strength of gases is a function of gap spacing and gas pressure; since the value of the latter varies with the ambient temperature, both the pressure and temperature must be recorded for breakdown results obtained with a fixed gap setting.

It should be emphasized that, when the breakdown voltages are determined for solid, liquid, and gas specimens, the gap length or specimen thickness must be stated in each case. Even when the value of the voltage breakdown strength is provided in the units of voltage per unit specimen thickness, the specimen thickness must still be specified, because the breakdown strength is a function of the specimen thickness.

Also, the dispersion in the voltage breakdown data requires some form of statistical analysis. Breakdown strength data ordinarily refer to a mean measured value on ten specimens. A low ratio (about 0.1) of the standard deviation to the mean value, derived from the ten measurements, is usually considered as an indicator of an acceptable probable error in the test results.

CONCLUDING REMARKS

The foregoing presentation of the measurement of conductivity, permittivity, and dielectric loss, and dielectric strength of electrical insulating materials has attempted to provide a concise cursory description of a number of the most common measurement techniques in use. Space limitations prevented a discussion on the various conduction and breakdown mechanism and their influence on the measured quantities. For a more in-depth discussion on the mechanisms involved and their determining inference on the measured quantities obtained with a variety of different test methods, the reader is referred to (2,18,20,42).

BIBLIOGRAPHY

1. R. Bartnikas, Dielectrics and insulators, in R. Dorf, (ed.), *The Electrical Engineering Handbook,* Boca Raton, FL: CRC/IEEE Press, 1997, chap. 55.
2. R. Bartnikas (ed.), *Engineering Dielectrics,* vol. IIB, *Electrical Properties of Solid Insulating Materials: Measurement Techniques,* STP926, Philadelphia: ASTM, 1987.
3. ASTM D257, Standard Test Methods for D-C Resistance or Conductance of Insulating Materials, *Annual Book of ASTM Standards,* vol. 10.01, Philadelphia, 1997.
4. *IEC Publication 93,* Methods of Test for Volume Resistivity and Surface Resistivity of Solid Electrical Insulating Materials.
5. ASTM D374, Standard Test Methods for Thickness of Solid Electrical Insulation, *Annual Book of ASTM Standards,* vol. 10.01, Philadelphia, 1997.
6. *Low Level Measurements,* 4th ed., Cleveland, OH: Keithley Instruments, 1993.
7. B. V. Hamon, An approximate method for deducing dielectric loss factor from direct current measurements, *Proc. IEE,* **99**: 151–155, 1952.
8. H. Block et al., Treatment of data in step-response dielectric relaxation measurements, *J. Chem. Soc., Faraday Trans. II,* **68**: 1890–1896, 1972.
9. H. St-Onge, Electrical conduction in 3-percent carbon filled polyethylene—Part I: Low field results, *IEEE Trans. Electr. Insul.,* **EI-11**: 20–27, 1976.
10. P. J. Hyde, Wide-frequency range dielectric spectrometer Part II, *Proc. IEE,* **117**: 1891–1901, 1970.
11. F. I. Mopsik, Precision time-domain dielectric spectrometer, *Rev. Sci. Instrum.,* **55**: 79–87, 1984.
12. A. M. Thompson, A bridge for the measurement of permittivity, Parts B and C, *Proc. IEE,* **103**: 705–709, 1955.
13. W. P. Harris, *Operators Procedures Manual for the Harris Ultra-Low Frequency Impedance Bridge,* National Bureau of Standards Report No. 9627, Washington, DC, 1968.
14. R. J. Kriegler and R. Bartnikas, Dielectric loss and current-voltage measurements in sodium-contaminated Si-SiO_2–Cr structures, *IEEE Trans. Electron Devices,* **ED-20**: 722–731, 1973.
15. J. Pugh, *4th Int. Conf. Dielectr. Mater. Meas. Appl.,* IEE Conf. Publ. No. 239, Lancaster, England, Sept. 10–13, 1984, pp. 247–249.
16. ASTM D150 Standard Test Methods for AC Loss Characteristics and Permittivity (Dielectric Constant) of Solid Electrical Insulating Materials, *Annual Book of ASTM Standards,* vol. 10.01, 1998.
17. H. J. Wintle and S. Kurylowicz, Edge corrections for strip and disc capacitors, *IEEE Trans. Instrum. Meas.,* **IM-34**: 41–47, 1985.
18. R. Bartnikas (ed.), *Engineering Dielectrics, vol. III, Electrical Insulating Liquids,* Monograph 2, ASTM, Philadelphia, 1994.
19. R. Bartnikas and K. D. Srivastava (eds.), *Power Cable Engineering,* Waterloo, Ont.: Sandford Fleming, 1987.
20. R. Bartnikas and E. J. McMahon (eds.), *Engineering Dielectrics, vol. I, Corona Measurement and Interpretation,* STP 669, ASTM, Philadelphia, 1979.
21. Tettex AG, Präzisions-Verlustfactor und Kapazitäts MeBbrücke Typ 2821, Prospekt 2821, Blatt 103, Zürich, 1980.
22. O. Petersons, A self-balancing high voltage capacitance bridge, *IEEE Trans. Instrum. Meas.,* **IM-13**: 216–224, 1964.
23. *Bridges / Standards,* Gen Rad Bulletin JN 4240-681, Gen Rad, Boston, MA.
24. P. Osvath and S. Widmer, A high-voltage high-precision self-balancing capacitance and dissipation factor-measuring bridge, *IEEE Trans. Instrum. Meas.,* **IM-35**: 19–23, 1986.
25. ASTM D1531. Test for Dielectric Constant and Dissipation Factor of Polyethylene by Liquid Displacement Procedure, *Annual Book of ASTM Standards, vol. 10.01,* 1997.
26. L. Hartshorn and W. H. Ward, The measurement of the permittivity and power factor of dielectrics at frequencies from 10^4 to 10^8 cycles per second, *J. IEE,* **79**: 597–609, 1936.
27. W. Reddish et al., Precise measurement of dielectric properties at radio frequencies, *Proc. IEE,* **118**: 255–265, 1971.
28. K. A. Buckingham and J. W. Billing, *3rd Int. Conf. on Dielectr. Meas. Appl.,* Birmingham, England, Sept. 10–13, 1979, pp. 392–395.
29. T. V. L. Parry, The measurement of permittivity and power factors of dielectrics at frequencies from 300 to 600 c/s, part III, *J. IEE,* **98**: 303–311, 1951.
30. S. Roberts and A. von Hippel, A new method for measuring dielectric constant and loss in range of centimeter waves, *J. Appl. Phys.,* **17**: 610–616, 1946.
31. W. B. Bridges, M. B. Klein, and E. Schweigh, Measurement of dielectric constant and loss tangent of thallium mixed halide crystals KRS-5 and KRS-6 at 95 GHz, *IEEE Trans. Microw. Theory Tech.,* **MTT-30**: 286–292, 1982.
32. ASTM D2520. Test Methods for Complex Permittivity of Solid Electrical Insuluating Materials at Microwave Frequencies and Temperatures to 1650°C, *Annual Book of ASTM Standards,* vol. 10.01, 1998.
33. W. B. Westphal, Distributed circuits, in A. von Hippel (ed.), *Dielectric Materials and Applications,* New York: Wiley, 1954, chap. 2, sect. A2.
34. T. W. Dakin and C. Works, Microwave dielectric measurements, *J. Appl. Phys.,* **18**: 789–796, 1947.
35. A. C. Lynch, Transmission methods for measurement of dielectric loss, *Conf. High Frequency Dielectr. Meas.,* Natl. Physical Laboratory, Teddington, England, March 27–29, 1972.
36. IEC Publication 377-2 , *Measurement of Permittivity and Loss at Frequencies above 300 MHz.*
37. A. H. Sharbough and S. Roberts, Dielectric measurement procedures, in K. Lark-Horowitz and V. A. Johnson (eds.), *Solid State Physics,* vol. VI, part B, New York: Academic Press, 1959, chap. 7, sect. 71.

38. W. Culshaw, A spectrometer for millimetre wavelengths, *Proc. IEE,* part IIA, **100**: 5–14, 1953.

39. J. E. Degenford, A quasi-optic technique for measuring dielectric loss tangents, *IEEE Trans. Instrum. Meas.,* **IM-17**: 413–417, 1968.

40. J. Chamberlain, Submillimetre-wave techniques, Conf. High Frequency Meas., Natl. Physical Laboratory, Teddington, England, March 27–29, 1972.

41. J. R. Birch, et al., An intercomparison of measurement techniques for the determination of the dielectric properties of solids at near millimeter wavelengths, *IEEE Trans. Microw. Theory Tech.,* **42**: 956–965, 1994.

42. J. K. Nelson, in R. Bartnikas and R. M. Eichhorn, (eds.), *Engineering Dielectrics, Vol. IIA, Electrical Properties of Solid Insulating Materials: Molecular Structure and Electrical Behavior,* STP 783, ASTM, Philadelphia, 1983.

43. S. Whitehead, *Dielectric Breakdown of Solids,* Oxford: Clarendon Press, 1953.

44. ASTM D149. Test Method for Dielectric Breakdown Voltage and Dielectric Strength of Electrical Insulating Materials at Commercial Power Frequencies, *Annual Book of ASTM Standards,* vol. 10.01, 1997.

45. IEC Publication 60, 243, parts 1–3, *Electric Strength of Insulating Materials—Test Methods.*

46. ASTM D877. Standard Test Method for Dielectric Breakdown Voltage of Insulating Liquids Using Disk Electrodes, *Annual Book of ASTM Standards,* vol. 10.03, 1997.

47. D1816. Standard Test Method for Dielectric Breakdown Voltage of Insulating Oils of Petroleum Origin Using VDE Electrodes, *Annual Book of ASTM Standards,* 1997. vol. 10.03. Also see VDE (Verband Deutscher Elektrotechniker) Specification 0370.

48. ASTM D3300. Standard Test Method for Dielectric Breakdown Voltage of Insulating Oils of Petroleum Origin under Impulse Conditions, *Annual Book of ASTM Standards,* vol. 10.03, 1997.

49. ASTM D2477. Standard Test Method for Dielectric Strength of Insulating Gases at Commercial Power Frequencies, *Annual Book of ASTM Standards,* vol. 10.03, 1997.

50. ASTM D3755. Test Method for Dielectric Breakdown Voltage and Dielectric Strength of Solid Electrical Insulating Materials under Direct Voltage Stress, *Annual Book of ASTM Standards,* vol. 10.02, 1997.

R. BARTNIKAS
IREQ/Institut de Recherche
d'Hydro-Québec